

Observed trends in ground-level O₃ in Monterrey, Mexico during 1993-2014: Comparison with Mexico City and Guadalajara

Iván Y. Hernández Paniagua^{1,2}, Kevin C. Clemitshaw³, and Alberto Mendoza^{1,*}

¹Escuela de Ingeniería y Ciencias, Tecnológico de Monterrey, Campus Monterrey, Av. Eugenio Garza Sada 2501, Monterrey, N.L., México, 64849.

²Centro de Ciencias de la Atmosfera, Universidad Nacional Autónoma de México, México.

³Department of Earth Sciences, Royal Holloway University of London, Egham, Surrey TW20 0EX, UK.

*Corresponding author: mendoza.alberto@itesm.mx

Keywords

Air quality, emissions inventory, odd oxygen, time series, wind-sector analysis

Abstract

Here, we present an assessment of long-term trends in O₃ and odd oxygen (O₃ + NO₂) at the industrial Monterrey metropolitan area (MMA) in NE Mexico. Diurnal amplitudes in O_x (AV_d) are used as a proxy for net O₃ production, which is influenced by the NO₂ photolysis rate. No significant differences in the AV_d are observed between weekends and weekdays, although the largest AV_d are observed at sites downwind of industrial areas. The highest O₃ mixing ratios are observed in spring, with minimum values in winter. The largest annual variations in O₃ are typically observed downwind of the MMA, with the lowest variations generally recorded in highly populated areas and close to industrial areas. A wind sector analysis of mixing ratios of O₃ precursors revealed that the dominant sources of emissions are located in the industrial regions within the MMA and surrounding area. Significant increasing trends in O₃ in spring, summer and autumn are observed depending on site location, with trends in annual averages ranging between 0.19 and 0.33 ppb yr⁻¹. Overall, during 1993 to 2014, within the MMA, O₃ has increased at an average rate of 0.22 ppb yr⁻¹ ($p < 0.01$), which is in marked contrast with the decline of 1.15 ppb yr⁻¹ ($p < 0.001$) observed in the Mexico City metropolitan area (MCMA) for the same period. No clear trend is observed during 1996 to 2014 within the Guadalajara metropolitan area (GMA).

1. Introduction

O₃ is a secondary air pollutant formed in the troposphere via the photo-oxidation of CO, methane (CH₄) and volatile organic compounds (VOCs) in the presence of NO and NO₂ (NO + NO₂ = NO_x) (Jenkin and Clemitshaw, 2000). The system of O₃ production is not linear, and is termed NO_x-limited, when O₃ production increases in response to increasing NO_x emissions, and termed VOC-limited when it responds positively to emissions of VOCs (Monks et al., 2015; Pusede et al., 2015). Tropospheric O₃ is of concern to policy makers due to its adverse impacts on human health, agricultural crops and

39 vegetation, and also due to its role as a greenhouse gas despite its relatively short lifetime of around
40 22.3 ± 3.0 days (Stevenson et al., 2006; IPCC, 2013; WHO, 2014; Lelieveld et al., 2015). As the
41 predominant source of OH, tropospheric O₃ controls the lifetime of CH₄, CO, VOCs, among many other
42 air pollutants (Revell et al., 2015). In polluted regions, increased levels of O₃ are prevalent during
43 seasons with stable high-pressure systems and intense photochemical processing of NO_x and VOCs
44 (Dentener et al., 2005; Xu et al., 2008) with downward transport from the stratosphere of lesser
45 importance (Wang et al., 2012). By contrast, the main removal processes for tropospheric O₃ are
46 chemical loss and dry deposition (Atkinson, 2000; Jenkin and Clemitshaw, 2000).

47

48 Tropospheric O₃ increased in the Northern Hemisphere (NH) during 1950-1980s due to rapid increases
49 in precursor emissions during the industrialisation and economic growth of Europe and North America
50 (NA) (Staehelin and Schmid, 1991; Guicherit and Roemer, 2000). Since the 1990s, reductions in O₃
51 precursor emissions in economically developed countries have resulted in decreases in tropospheric O₃
52 levels (Schultz and Rast, 2007; Butler et al., 2012; Pusede et al., 2012), however, in some regions,
53 increases in O₃ have also been reported. For instance, from an analysis of O₃ data from 179 urban sites
54 over France during 1999-2012, Sicard et al. (2016) reported an increasing trend in the annual averages
55 of 0.14 ± 0.19 ppb yr⁻¹, and in the medians of 0.13 ± 0.22 ppb yr⁻¹, attributed to long-range transport and
56 reduced O₃ titration by NO due to reductions in local NO_x emissions. However, Sicard et al. (2016) also
57 reported during the same period that at 61 rural sites, O₃ decreased in the annual averages by $0.12 \pm$
58 0.21 ppb yr⁻¹, and in the medians by 0.09 ± 0.22 ppb yr⁻¹.

59

60 In the US and Canada, O₃ levels have decreased substantially at different metrics during the last two
61 decades in response to more stringent emission controls focused on on-road and industrial sources. In
62 the Greater Area of Toronto from 2000 to 2012, O₃ levels decreased at urban sites by approximately 0.4
63 % yr⁻¹, and at sub-urban sites by approximately 1.1 % yr⁻¹, as a consequence of a reduction in the mid-
64 day averages of NO₂ of 5.8 - 6.4 % yr⁻¹, and in the VOC reactivity of 9.3% yr⁻¹ (Pugliese et al., 2014).
65 Emission estimates suggest an overall national scale decrease during 1980-2008 in US NO_x and VOCs
66 emissions of 40 % and 47 %, respectively, with city-to-city variability (EPA, 2009; Xing et al., 2013).
67 Lefohn et al. (2010) reported that for 12 US major metropolitan areas, the O₃ US EPA exposure metrics
68 of the annual 2nd highest 1-h average, and the annual 4th highest daily maximum 8-h average, decreased
69 during 1980-2008 at 87 % and 71 % of the monitoring sites evaluated, respectively. However, Lefohn et
70 al. (2010) observed an increase in the lower- and mid-O₃ mixing ratios in response to decreased titration
71 by NO. More recently, Simon et al. (2015) assessed changes in the 1-h average O₃ mixing ratios at
72 around 1400 sites across the US between 1998-2013, using the 5th, 25th, 50th, 75th, 95th percentiles, and
73 the maximum daily 8-h average. Overall, Simon et al. (2015) observed increases at the lower end of the
74 O₃ data distribution of 0.1-1 ppb yr⁻¹, mostly in urban and sub-urban areas, whereas O₃ decreased at the
75 upper end of the data distribution between 1-2 ppb yr⁻¹ at less urbanised areas. Such changes were

associated with the implementation of control strategies within the US to abate peak O₃ mixing ratios, as the NO_x SIP Call and, tighter point and vehicle emission standards.

In Mexico, studies of long-term trends in O₃ have focused on the Mexico City Metropolitan Area (MCMA) (Molina and Molina, 2004; Jaimes et al., 2012; Rodríguez et al., 2016), with reports of a decrease in O₃ annual averages of ca. 33 % during the last two decades (Parrish et al., 2011; SEDEMA, 2016a). O₃ has received less consideration at other large metropolitan areas, where Mexican air quality standards are frequently exceeded (Table 1). Indeed, since 2000, recorded O₃ mixing ratios have exceeded Mexican official standards for O₃ 1-h average (110 ppb) and 8-h running average (80 ppb) by more than 50 % at the Guadalajara metropolitan area (GMA, the second most populated city) and at the Monterrey metropolitan area (MMA, the third most populated city (INE, 2011; SEMARNAT, 2015). To date, only Benítez-García et al. (2014) have addressed changes in ambient O₃ at the GMA and MMA during 2000-2011, reporting an increase in O₃ annual averages of around 47 % and 42 %, respectively. However, it should be noted that the ordinary linear regression analysis used by Benítez-García et al. (2014) may be biased by extreme values and is therefore not suitable to determine O₃ long-term trends with significant confidence.

To improve air quality, the Mexican government has introduced several initiatives to reduce primary pollutants emissions, with emission estimates reported in the Mexican National Emissions Inventories (NEI). The NEI suggest that from 1999 to 2008, anthropogenic NO_x emissions decreased at the MCMA by 3.8 % yr⁻¹, but increased at the GMA and the MMA by 1.9 % yr⁻¹, and by 4.0 % yr⁻¹, respectively (Fig. S1) (SEMARNAT, 2006, 2011, 2014). These NEI NO_x emission estimates agree with the decrease for the MCMA of 1.7 % yr⁻¹ in the NO₂ vertical column density during 2005-2014 reported by Duncan et al. (2016), but disagree for the GMA and the MMA where decreases of 2.7 % yr⁻¹ and of 0.3 % yr⁻¹, respectively, are reported. Similarly, Boersma et al. (2008) observed that NO_x emissions over Mexico derived from NO₂ satellite observations were higher by a factor of 1.5 - 2.5 times than bottom-up emission estimates, which were lower by 1.6 - 1.8 times than data reported in the NEI 1999-base year. The NEI anthropogenic VOCs emissions estimates suggest a decrease at the MMA by 0.2 % yr⁻¹, but increases at the MCMA and at the GMA by 2.7 % yr⁻¹ and by 3.2 % yr⁻¹, respectively (Fig. S1) (SEMARNAT, 2006, 2011, 2014). However, as for NO_x, NEI trends in VOCs disagree with existing reports for average VOCs decreases within the MCMA (Arriaga-colina et al., 2004; Garzón et al., 2015).

Local authorities have developed local emission inventories for the MCMA and the MMA, although only for the MCMA the inventories have been compiled with a frequency of two years since 1996 (SEDEMA, 1999, 2001, 2003, 2004, 2006, 2008, 2010, 2012, 2014, 2016b; SDS, 2015). The accuracy of the MCMA emission inventories has been also assessed during several field campaigns. For instance, during the MCMA 2002-2003 campaign, Velasco et al. (2007) observed an overestimation in the 1998 inventory for VOCs emissions of alkenes and aromatics, but an underestimation in the contribution of some alkanes.

114 By contrast, for the 2002 MCMA inventory, Lei et al. (2007) reported an underestimation in the VOCs
115 total emissions of around 65 %, based on a simulation of an O₃ episode occurred in 2003 within the
116 MCMA. Therefore, since these emission estimates are used to predict future air quality, and to design
117 clean air policies, it is imperative to examine the results of the policies implemented to control emissions
118 of O₃ precursors.

119
120 To our knowledge, no previous study has address trends in O₃ and odd oxygen in urban areas of Mexico.
121 In this study, we describe trends in ground-level O₃ within the MMA, and its response to changes in
122 precursor emissions during 1993-2014. Long-term and high-frequency measurements of O₃ were
123 recorded at 5 air quality monitoring stations evenly distributed within the MMA. In order to better assess
124 photo-chemical production of O₃, odd oxygen defined as ([O_x] = [O₃] + [NO₂]) was also considered, as
125 O₃ and NO₂ are rapidly interconverted. Diurnal and annual cycles of O₃ and O_x are used to interpret net
126 O₃ production within the MMA. We show that air mass origin influences strongly the O₃ annual increases.
127 The trends in O₃, O_x and precursor emissions are compared with those observed within the MCMA and
128 GMA. Finally, we describe that NEI emission estimates for NO_x and VOCs disagree in the trend
129 magnitudes with ground-based NO_x and VOCs measurements made at the urban areas studied here.

130
131 This paper is organised as follows: Section 2 presents the data quality and methodology used to derive
132 the different trends presented. Section 3 describes in detail the O₃ and O_x diurnal and annual cycles,
133 and, annual and seasonally averaged trends. Section 4 discusses the origin of the O₃ and O_x diurnal
134 variations and trends in the light of changes in precursor emissions. Finally, Section 5 provides some
135 conclusions regarding the trends observed at the studied urban areas.

136

137 **2. Methodology**

138 **2.1 Monitoring of O₃ in the Monterrey Metropolitan Area (MMA).**

139 The MMA (25°40'N, 100°20'W) is located around 720 km N of Mexico City, some 230 km S of the US
140 border in the State of Nuevo Leon (Fig. 1a). It lies at an average altitude of 500 m above sea level (m
141 asl) and is surrounded by mountains to the S and W, with flat terrain to the NE (Fig. 1b). The MMA is the
142 largest urban area in Northern Mexico at around 4,030 km², and is the third most populous in the country
143 with 4.16 million inhabitants, which in 2010, comprised 88 % of the population of Nuevo Leon State
144 (INEGI, 2010). It is the second most important industrial area in Mexico and has the highest gross
145 domestic product per capita (Fig. 1c). Although the weather changes rapidly on a daily time-scale, the
146 climate is semi-arid with an annual average rainfall of 590 mm, and an annual average temperature of
147 25.0°C with hot summers and mild winters (ProAire-AMM, 2008; SMN, 2016).

148

149 Within the MMA, tropospheric O₃, 6 additional air pollutants (CO, NO, NO₂, SO₂, PM₁₀, and PM_{2.5}) and 7
150 meteorological parameters (wind speed (WS), wind direction (WD), temperature (Temp), rainfall, solar
151 radiation (SR), relative humidity (RH) and pressure) have been monitored continuously, with data

summarised as hourly averages, since November 1992 at 5 stations that form part of the Integral Environmental Monitoring System (SIMA) of the Nuevo Leon State Government (Table 2; SDS, 2016). From November 1992 to April 2003, and in accordance with EPA, EQOA-0880-047, Thermo Environmental Inc. (TEI) model 49 UV photometric analysers were used to measure O₃ with stated precision less than ± 2 ppb O₃ and a detection limit of 2 ppb O₃. Similarly, in accordance with RFNA-1289-074, TEI model 42 NO-O₃ chemiluminescence detectors were used to measure NO-NO₂-NO_x with stated precision less than ± 0.5 ppb NO, and a detection limit of 0.5 ppb NO. In May 2003, replacement TEI model 49C O₃ and model 42C NO-NO₂-NO_x analysers were operated as above, with stated precision better than ± 1 ppb O₃ and ± 0.4 ppb NO, respectively, and detection limits of 1 ppb O₃ and 0.4 ppb NO, respectively. To rule out instrumentation influences on the determined air pollutants trends, long-term trends based on annual averages were compared with those derived using 3-yr running averages, in accordance with Parrish et al. (2011) and Akimoto et al. (2015) (Supplementary Information S1.1; Fig. S2). Calibration, maintenance procedures and quality assurance/quality control (QA/QC) followed protocols established in the Mexican standards NOM-036-SEMARNAT-1993 and NOM-156-SEMARNAT-2012. The SIMA dataset has been validated by the Research Division of Air Quality of the Secretariat of Environment and Natural Resources (SEMARNAT). The monitoring of O₃ and other air pollutants at the MCMA and the GMA is detailed in the Supplementary Information S1.2-3.

169

170 **2.2 NEI data**

NEI data for estimated NO_x and VOCs emissions for the 1999-, 2005- and 2008-base years were obtained from the SEMARNAT website (<http://sinea.semarnat.gob.mx>). The data comprised emission sources (mobile, point, area and natural) and air pollutants (NO_x, VOCs, SO_x, CO, PM_{2.5} and PM₁₀), at national, state and municipality scales. The NEI emission estimates are developed in accordance with the Manual for the Emission Inventories Program of Mexico (Radian, 2000), which is based on the US EPA AP-42 emission factors categorisation (EPA, 1995). The emission factors are regionalised for each Mexican state, based upon on-site measurements and survey information. Updates to the emission factors have been conducted for each released NEI, although no changes in the methodology were implemented between the 1999- and 2008-base years. Overall, the mobile emissions were estimated using the MOBILE6-Mexico model (EPA, 2003). The emissions from point sources were derived using the annual operation reports submitted to the Environment Ministry. The emissions from area sources were obtained using the categorisation of Mexican area sources and the regionalised AP-42 emission factors.

184

The MCMA emissions inventories have been developed with a 2-year frequency since 1996, and were obtained from the MCMA Environment Secretariat website (<http://www.aire.cdmx.gob.mx/>). The methodology used to construct the MCMA inventories estimates is consistent with that used in the NEI (SEDEMA, 2016a), which is based on the AP-42 EPA emission factors. However, more speciated emission factors have been developed in each released version, considering updates in the local

190 industrial activity, survey information and field measurement campaigns. To date, the only significant
191 change in the methodology is the replacement of the Mobile6-Mexico model with the MOVES model to
192 obtain the 2014-base year mobile emissions (SEDEMA, 2016b). As for the MCMA inventories, more
193 speciated emission factors than those contained in the NEI were developed to produce the MMA
194 emissions inventory 2013-base year (SDS, 2015), although, estimates of mobile emissions were
195 obtained with the Mobile6-Mexico model (EPA, 2003).

196

197 **2.3 Analytical methods**

198 SIMA, SIMAT (Atmospheric Monitoring System of the MCMA) and SIMAJ (Atmospheric Monitoring
199 System of the GMA) instrumentation recorded O₃ data every minute, which were then validated and
200 archived as 1-h averages. Total SIMA O₃ data capture by year and site are shown in Fig. S3. Data
201 capture averaged during 1993-2014 ranged from 82.6 % at GPE to 93.3 % at SNB, with data capture
202 <50 % during 1998-2000 at GPE, in 1998 at SNN, and in 1999 at OBI. A threshold of 75% data capture
203 was defined to consider data valid and representative (ProAire-MMA, 2008; Zellweger et al., 2009;
204 Wilson et al., 2012). All data were processed with hourly averages used to determine daily averages,
205 which were used to calculate monthly averages, from which yearly averages were obtained.

206

207 **2.4 Data analysis methods**

208 The SIMA, SIMAT and SIMAJ O₃ data sets were analysed extensively using the *openair* package v. 1.1-
209 4 (Carslaw and Ropkins, 2012) for R software v. 3.1.2 (R Core Team, 2013). In this study, the *openair*
210 functions *windRose*, *timeVariation* and *TheilSen* were used to analyse air pollution data. Briefly, the
211 *windRose* summarises wind speed and wind direction by a given time-scale, with proportional paddles
212 representing the percentage of wind occurrence from a certain angle and speed range. The *timeVariation*
213 function was used to obtain normalised daily cycles by season, and weekly cycles, with the 95 %
214 confidence intervals in the cycles calculated from bootstrap re-sampling, which accounts for better
215 estimations for non-normally distributed data (Carslaw, 2015). Finally, long-term trends of air pollutants
216 at the MCMA, GMA and MMA were computed with the *TheilSen* function, which is based on the non-
217 parametric Theil-Sen method (Carslaw, 2015; and references therein). The Theil-Sen estimate of the
218 slope is the median of all slopes calculated for a given *n* number of *x,y* pairs, while the regression
219 parameters, confidence intervals and statistical significance are determined through bootstrap re-
220 sampling. It yields accurate confidence intervals despite the data distribution and heteroscedasticity, and
221 is also resistant to outliers.

222

223 The trends computed with *openair* were contrasted with those calculated using the MAKESENS 1.0
224 macro (Salmi et al., 2002) as follows. Firstly, the presence of a monotonic trend was tested with the non-
225 parametric Mann-Kendal test. For the MCMA, GMA and MMA, the available yearly data are *n*>10, hence
226 positive values in the *Z* parameter correspond to positive trends and vice-versa for negative values of *Z*.
227 The significance of the estimated trend was tested at $\alpha=0.001$, 0.01, 0.05 and 0.1 using a two-tailed test.

Secondly, slopes of linear trends were calculated with the non-parametric Sen's method, which assumes linear trends, with a Q slope and a B intercept. To calculate Q , first the slopes of all data values were calculated in pairs, with the Sen's estimator slope as the median of all calculated slopes. Finally, $100(1-\alpha)$ % two-sided confidence intervals about the slope estimate were obtained based on a normal distribution. Comparisons of estimated trends from both approaches are shown in the Supplementary information S1.4 (Fig. S4).

The O_3 and other air pollutant time-series were decomposed into trend, seasonal and residual components using the Seasonal-Trend Decomposition technique (STL; Cleveland et al., 1990). STL consists of two recursive procedures: an inner loop nested inside an outer loop, assuming measurements of x_i (independent) and y_i (dependent) for $i = 1$ to n . The seasonal and trend components are updated once in each pass through the inner loop; each complete run of the inner loop consists of $n_{(i)}$ such passes. Each pass of the outer loop consists of the inner loop followed by a computation of the robustness weights, which are used in the following run of the inner loop to minimise the influence of transient and aberrant behaviour on the trend and seasonal components. The initial pass of the outer loop is performed with all robustness weights equal to 1, followed by $n_{(o)}$ passes of the outer loop. The Kalman Smoother (KS) was used to provide minimum-variance, unbiased linear estimations of observations and to impute missing data to satisfy the STL (Reinsel, 1997; Durbin and Koopman, 2012; Carslaw, 2015). Overall, statistical seasonal auto-regressive and moving averages with annual seasonal components were employed. Statistical analyses were carried out with SPSS 19.0.

In order to carry out seasonal analyses of data, seasons were defined according to temperature records in the NH, as described previously (Hernandez-Paniagua et al., 2015): winter (December-February), spring (March-May), summer (June-August) and autumn (September-November). Wind-sector analyses of data were performed by defining 8 wind sectors each of 45° starting from $0^\circ \pm 22.5^\circ$. The lower bound of each sector was established by adding 0.5° to avoid data duplicity. Data were assigned to a calm sector when wind speed was $\leq 0.36 \text{ km h}^{-1}$ (0.1 m s^{-1}). To assess regional transport, air mass back-trajectories (AMBT) were calculated using the HYSPLIT model v.4 (NOAA Air Resources Laboratory (ARL); Stein et al., 2015), with the Global NOAA-NCEP/NCAR reanalysis data files on a latitude-longitude grid of 2.5° , downloaded from the NOAA ARL website (<http://ready.arl.noaa.gov/HYSPLIT.php>). HYSPLIT frequency plots of 96-h AMBT were constructed for every 6 h during the year 2014 with an arrival altitude of 100 m above ground level.

3. Results

3.1 Wind occurrence at the MMA

The MMA is highly influenced by anti-cyclonic easterly air masses that arrive from the Gulf of Mexico, especially during spring and summer (Fig. S5). Figure 2 shows the frequency count of 1-h averages of wind direction by site and season within the MMA during 1993-2014. At all sites, apart from OBI, the

predominant wind direction is clearly E, which occurs between 35-58 % of the time depending on season. Easterly air masses are augmented by emissions from the industrial area E of the MMA, which are transported across the urban core and prevented from dispersing by the mountains located S-SW of the MMA. On average, the highest wind speeds are observed during summer at all sites. By contrast, calm winds of $\leq 0.36 \text{ km h}^{-1}$ (0.1 m s^{-1}) occurred less than 2 % of the time at all sites, most frequently in winter, and least frequently in summer.

272

273 **3.2 Time-series in O₃ and O_x recorded within the MMA during 1993-2014**

274 Within the MMA, the highest O₃ mixing ratios (1-h averages) are typically observed between April-
275 September, whereas the lowest values are usually recorded between December-January (winter) (Fig.
276 S6). Table S1 summarises the minimum, maximum, average (mean) and median hourly O₃ mixing ratios
277 recorded during 1993-2014. The highest O₃ mixing ratios recorded were 186 ppb at GPE in 1997, 146
278 ppb at SNN in 2004, and 224 ppb at SNB in 2001. At OBI and STA, the highest O₃ mixing ratios were
279 both recorded on June 2, 1993: 182 ppb at 12:00 CDT at OBI, and 183 ppb at 13:00 CDT at STA, during
280 the occurrence of E winds. Note that all times below are given in CDT. Annual O₃ averages varied from
281 14 ± 14 ppb at OBI in 2001 to 32 ± 23 ppb at SNB in 1993, whereas O₃ annual medians ranged from 10
282 ppb at OBI in 2001 to 28 ppb at SNN in 1993.

283

284 Reaction with O₃ rapidly converts NO to NO₂, and therefore mixing ratios of odd oxygen ($\text{O}_x = \text{O}_3 + \text{NO}_2$)
285 were calculated to account for O₃ stored as NO₂ for each hour during 1993-2014 at the 5 sites within the
286 MMA (Table S2; Fig. S7). Minimum values of O_x ranged from 2 ppb, observed at all sites mostly during
287 1993-2014 to 13 ppb at OBI in 2007. Maximum values of O_x ranged from 99 ppb at SNN in 2002, to 330
288 at OBI in 1993. O_x annual averages varied from 23 ± 17 ppb at SNN in 2002 to 51 ± 27 ppb at OBI and
289 at STA in 2001 and 2006, respectively, whereas O_x annual medians ranged from 21 ppb at SNB and
290 SNN, in 2001 and 2002, respectively, to 46 ppb at OBI and STA in 2001 and 2006, respectively. It is
291 clear that the highest O₃ and O_x mixing ratios were recorded when control of precursor emissions of
292 VOCs and NO_x were less stringent than subsequently.

293

294 **3.2 Diurnal variations in O₃ and O_x within the MMA**

295 Here, O₃ diurnal variations were used to assess changes in the net O₃ production. Figure 3 shows daily
296 profiles by season of O₃, O_x, NO, NO₂, NO_x, and SR averaged over the 5 sites within the MMA. O₃
297 generally dips during the morning rush hour due to titration with NO and mirrors the increase in NO₂,
298 which occurs around 07:00 in spring and summer, and around 08:00 in autumn and winter. The 1-h
299 difference in the O₃ dip derives from the change to daylight saving time during spring and summer. O₃
300 generally peaks during the enhanced photochemical period, around 13:00 in spring, 12:00 in summer
301 (co-incident with SR), and about 14:00 in autumn and winter. Similar profiles are observed for O₃ in all
302 seasons, being negatively correlated with NO₂ ($r=0.93$ (winter) to $r=0.97$ (summer) ($p<0.05$)), due to the
303 rapid photolysis of NO₂. Diurnal cycles of O_x behave as O₃, with lowest values before the morning rush

hour and the largest between midday (summer) and 15:00 (winter). During daytime, O_x and O_3 diurnal cycles are strongly correlated in all seasons, ranging from $r=0.97$ in winter to $r=0.99$ in autumn ($p<0.05$), which suggests net O_3 production during daytime.

O_x amplitude values (AV_d) derived from normalised daily cycles were used as a proxy to assess differences in the net O_3 production from site-to-site within the MMA. The normalised daily cycles were constructed by subtracting daily averages from hourly averages. Figure 4 shows normalised O_x daily cycles. The lowest AV_d s in O_x occur in winter consistent with reduced SR and low photolysis rates, with the largest values observed in summer. It is clear that during the year, the largest AV_d s are recorded at sites downwind of industrial emission sources, in particular at STA, while the lowest AV_d s are observed at sites upwind. The larger AV_d s at downwind sites are interpreted to indicate higher net O_3 production, derived from the occurrence of photochemical processed air masses from the E sector. The AV_d s at upwind sites are less affected by emissions from the MMA, and especially the industrial area.

3.3. Annual cycles of O_3 and O_x within the MMA

Annual variations in O_3 and O_x are correlated positively with the seasonality of temperature, RH and SR (Camalier et al., 2007; Zheng et al., 2007). Annual averages cycle for those meteorological variables, O_3 and O_x were constructed by averaging monthly averages for the same month during the studied period. Figure 5a shows that O_3 exhibits the maxima during spring and minima in winter, with a downward peak in early autumn, behaviour characteristic of tropospheric O_3 in the NH. O_x peaks in spring and dips in summer, although it is evident that NO_x emissions lead to apparently similar O_x levels in winter and spring despite the decrease in O_3 levels. A correlation analysis among monthly averages for both O_3 and O_x with temperature, rainfall, RH and SR, revealed that the strongest relationship was between O_3 and SR ($r= 0.72$, $p<0.001$; Fig. 5a), with relationship evident with O_x .

The seasonal amplitude value (AV_s) provide insight into inter-annual variations in net O_3 production in response to changes in precursor emissions, meteorology, and O_3 chemistry. The seasonal cycles in O_3 during 1993-2014 were determined by filtering monthly averages with the STL technique (Cleveland et al., 1990) (Fig. S8). O_3 AV_s s were calculated as the difference peak-to-trough (spring peak). An average O_3 AV_s of 15.1 ± 2.97 (1σ) ppb was calculated from 1993 to 2014 within the MMA, with the lowest O_3 AV_s of 10.3 ppb determined in 1998, and the largest O_3 AV_s of 19.0 ppb observed in 2014. Figure 5b shows that O_3 AV_s decreased significantly at all sites between 1993 and 1997-1998, at rates from 0.78 ppb O_3 yr^{-1} at GPE to 2.28 ppb O_3 yr^{-1} at SNN (Fig. 5c). O_3 AV_s s increased constantly ($p<0.05$) at all sites since 1998, ranging from 0.90 ppb O_3 yr^{-1} at GPE to 0.75 ppb O_3 yr^{-1} at SNN. O_x AV_s s exhibited no discernible trends at all sites for the whole studied period, although, SNN show a significant ($p<0.05$) decline during 1993-2001 (1.5 ppb yr^{-1}) and at STA show an increase during 2004-2010 (1.3 ppb yr^{-1}). The trends in O_x follow those observed for NO_x at SNN and STA during 1993-2014, which indicates that nearby industrial emissions have a significant contribution on the observed O_x levels within the MMA.

342
343
344
345
346
347
348
349
350
351
352
353
354
355
356
357
358
359
360
361
362
363
364
365
366
367
368
369
370
371
372
373
374
375
376
377
378
379

3.4. Long-term trends in O₃ and O_x within the MMA during 1993-2014

Quantifying the absolute changes in ground-level O₃ in response to trends in its precursor emissions is crucial to evaluate the impacts of air quality control (Parrish et al., 2009; Simon et al., 2015). The growing economy within the MMA has increased O₃ precursor emissions from point and area sources, due to the limited emissions control programs (INEGI, 2015; SDS, 2015). Moreover, predominant E-SE winds throughout the year transports primary pollutants and their oxidised products downwind from the industrial area, which can offset reductions in emissions from other sources. Here, to characterise changes in net O₃ production during 1993-2014 within the MMA in response to changes in its precursor emissions, long-term trends for daytime (06:00-18:00 CDT) O₃ and O_x measurements were derived by averaging data in seasonal periods. Seasonal averaging was used to minimise variability inherent in longer-term averages and the de-seasonalisation process avoids confounding overall trends, especially when seasons exhibit opposite trends. (Parrish et al., 2009).

Figure 6 shows seasonal trends in O₃ within the MMA, and Table 3 summarises the parameterisation of the trends. Significant increases ($p<0.1$) in O₃ are observed at all sites, apart from STA, in spring and summer, while in autumn, O₃ increases significantly only at SNN and SNB. The increases in O₃ range from 0.26 ppb yr⁻¹ in spring at OBI to 0.47 ppb yr⁻¹ in summer at SNN. Overall, the lowest O₃ growth rates are observed at the urban background GPE site, whereas the largest ones are at the industrial SNN site. It is worth noting that only SNN and OBI exhibit significant increases in autumn, despite a decrease in the frequency of high wind speeds (>20 km h⁻¹). The existence of significant trends at all sites during spring-summer, except for OBI, is consistent with the downwind transport of industrial emissions and the high frequency of photochemical processed air masses with NE-S-SE origin, where the industrial area is located (Fig. S9).

Seasonal trends in O_x are shown in Fig. 7, with the parameters of the trends listed in Table 3. Consistent with the seasonal O₃ trends observed, significant increases ($p<0.1$) in O_x within the MMA are determined in spring at all sites except for STA, and range from 0.02 ppb yr⁻¹ at OBI to 0.67 ppb yr⁻¹ at SNB. It is worth noting that the industrial SNN and SNB sites show significant increases in O_x in all seasons, with the lowest growth rates in winter and the largest in summer and spring, respectively. Moreover, STA exhibits the only significant decrease in O_x of 0.63 ppb yr⁻¹ during winter. As for O₃, the O_x increasing trends are consistent with the transport of primary emissions during the high occurrence of NE-E-SE air masses at WS >10 km h⁻¹, which is highlighted during the photochemical season (April-September). Furthermore, the small shift in wind direction at STA to NW during winter coincides with the only observed decrease in net O₃ production within the MMA, which confirms that O₃ precursors are emitted E of the MMA. This also makes evident that increasing upwind industrial emissions have offset reductions in emissions from on-road sources as revealed by the decline in NO_x evident at OBI.

3.5 Comparison of MMA O₃ and O_x weekly profiles with those at MCMA and GMA

O₃ production varies from city-to-city in response to local NO_x and VOCs emissions. Assessment of weekly profiles of O₃ and O_x may provide insights of the geographic response in net O₃ production to diurnal variations in precursor emissions. Hourly O₃ and O_x averages were used to construct weekday and weekend average profiles for the MCMA from 1993 to 2014, and for the GMA from 1996 to 2014. Figure 8 compares weekly O₃ and O_x profiles by season within the MMA with those for the MCMA and GMA. In each case, and consistent with observations in other major urban areas of NA, the lowest O₃ mixing ratios occur during the morning rush hour due to O₃ titration with NO emitted from on-road sources, whereas peak values of O₃ are apparent after mid-day during periods of enhanced SR (Stephens et al., 2008; Jaimes-Palomera et al., 2016). It should be noted that the peak value of O₃ for the GMA in winter and spring occurs an hour or so earlier than for the MMA and MCMA, which is consistent with higher VOC/NO_x emissions ratios at the GMA (Kanda et al., 2016). As might be anticipated, larger AV_d of 76.9 ± 1.6 ppb O₃ are observed for the MCMA than for the GMA (46.1 ± 1.0 ppb O₃) and MMA (37.6 ± 0.4 ppb O₃), related to the levels of emissions of the O₃ precursors. The O_x profiles show a trough during the morning rush hour and a peak between 12:00 and 14:00 at all urban areas. Despite large variations between weekday and weekend NO_x mixing ratios at the 3 urban areas as shown in Fig. 8, no significant differences ($p>0.05$) in O₃ and O_x are observed at any of the metropolitan areas between O₃ and O_x weekends and weekdays AV_{ds}.

Stephens et al. (2008) suggested that the most plausible explanation for the lack of weekend O₃ effect at MCMA during 1987-2007 is a simultaneous decrease in NO_x and VOCs emissions during weekends, since the sole decrease in NO_x emissions under VOC-limited conditions would lead to an increase in O₃ not observed. Similarly, a VOC-limited O₃ production regime was reported for the MMA by Sierra et al. (2013), whereas Kanda et al. (2016) reported that at the GMA the O₃ production lies in the region between VOC- and NO_x-sensitivity. Therefore, it can be suggested that simultaneous decreases in NO_x and VOCs emissions during weekends at the GMA and MMA explain the similar behaviour in O₃ and O_x as at the MCMA. Moreover, a change to a NO_x-limited O₃ production regime during weekends at the three urban areas seems unlikely, since this would result in lower O₃ levels during weekends, which is not observed at any of the studied urban areas (Torres-Jardon et al., 2009). Wolff et al. (2013) observed at several urban areas in the US similar O₃ levels during weekdays and weekends despite lower O₃ precursor emissions over weekends. Furthermore, the number of sites in the US that exhibited a weekend effect decreased from ca. 35 % to less than 5 % from 1997-1999 to 2008-2010, which was attributed to an increase in the VOC/NO_x emission ratio derived from a greater decline in NO_x than in VOCs emissions, mostly driven by reductions from on-road sources.

3.6 Long-term trends at MCMA, GMA and MMA from 1993 to 2014

The high mixing ratios of O₃ observed typically at the 3 largest urban areas in Mexico have motivated the introduction of control strategies to decrease emissions of the O₃ precursors, NO_x and VOCs. The

success of the control strategies implemented can be evaluated by assessing trends in O_3 and O_x . As for the MMA, seasonal trends in O_3 and O_x within the MCMA and GMA were calculated from daytime measurements. Figure 9 shows a comparison of inter-annual trends in O_3 and O_x at the 3 urban areas in Mexico, and Table 4 lists the parameters of the trends. Overall, during 1993-2014, daytime O_3 at the MCMA decreased significantly ($p<0.05$) by 1.15 ppb yr^{-1} ($2.04 \% \text{ yr}^{-1}$), and increased at the MMA by 0.22 ppb yr^{-1} ($0.84 \% \text{ yr}^{-1}$); at the GMA no discernible trend was observed during 1996-2014. For daytime O_x at the MCMA and GMA during the same periods, significant decreases ($p<0.05$) of 1.87 and 1.46 ppb yr^{-1} were determined, respectively, while the MMA does not exhibit a significant change. At the MCMA, the overall trends in O_3 and O_x are strongly driven by their wintertime decreases of 1.62 and 2.47 ppb yr^{-1} , respectively; whereas at the MMA, the annual growth in O_3 is driven by increases in spring and summer of 0.32 and 0.27 ppb yr^{-1} , respectively. Although, at the MMA, an increase in O_x of 0.28 ppb yr^{-1} is observed only during summer, the overall O_x trend is strongly affected by the non-significant trends in the other seasons. It is worth nothing that at the GMA, the overall decrease in O_x of 1.46 ppb yr^{-1} is similar for all seasons, which range between 1.40 ppb yr^{-1} (autumn) and 1.89 ppb yr^{-1} (spring).

The overall trends in net O_3 production during 1993-2014 at the MCMA and GMA are consistent with the significant ($p<0.05$) annual decreases in NO_x of 1.21 and 1.25 ppb yr^{-1} , respectively (Fig. 10). By contrast, while average NO_x levels have increased annually at the MMA at 0.33 ppb yr^{-1} ($p<0.05$), the average net O_3 production has remain steady. Either the non-linear response in O_x to the changes in NO_x in an environment of high NO_x mixing ratios ($>60 \text{ ppb}$) displace the chemical equilibrium to favour NO as the dominant component of NO_x which does not account for the levels of O_x (Clapp and Jenkin, 2001). Or the O_x trends derived from the combined data set for the MMA do not represent local observed trends, because a compensating effect between O_x reductions and increases.

3.7 Compliance with the 1-h and 8-h Mexican Standards for O_3 within the MMA

Between 1993 and 2014, there were two official standards for maximum permitted mixing ratios of O_3 in Mexico: i) a running 8-h average of 80 ppb , not to be exceeded more than 4 times per calendar year, and ii) a 1-h average of 110 ppb (NOM-020-SSA1-1993). Since 19 Oct 2014, the maximum permitted O_3 levels were lowered to a running 8-h average of 70 ppb and a 1-h average of 95 ppb , (NOM-020-SSA1-2014). However, because both standards are applicable for whole calendar years, the old permitted O_3 levels were used in this study to determine the number of annual exceedances to both O_3 standards. Figure 11 shows that within the MMA, the O_3 1-h average and the running 8-h standards were frequently exceeded (INE, 2011; SEMARNAT, 2015). The largest number of exceedances occurs at STA, followed by SNB, GPE and OBI, whereas the fewest breaches are observed at SNN markedly since 2004. However, there have been 3 periods of clear decreased exceedances at all sites (except STA in 2014), during 1994-1995, 1999-2000, and 2012-2013, which are consistent with marked changes in the national GDP during economic recessions in Mexico (Fig. S10a). However, although, national GDP exhibits a

notable decrease during the 2008-2009 global economic recession, only in 2009 do the O₃ annual exceedances within the MMA seem to follow (Fig. S10b).

Therefore, if O₃ levels continue to increase within the MMA, as determined in the long-term trend assessment, an increase also in peak O₃ mixing ratios is likely to occur. Hence, to analyse changes in peak O₃, daily maxima 1-h averages from 1993 to 2014 were used to determine seasonal trends in peak levels. Figure 12 shows trends in 1-h daily maxima and Table 5 list the parameters of the trends. Daily maxima O₃ 1-h averages have increased significantly ($p < 0.05$) in spring and summer at all sites, except for STA, and also in autumn at the industrial sites SNN and SNB. The largest increases in the daily maxima are seen at SNN, where similar increases between 0.85 and 0.93 ppb yr⁻¹ are determined between spring and autumn. SNB exhibits slightly lower growth rates in spring and summer, but a large difference in autumn. We have shown that predominantly E-SE winds transport photochemically processed air masses to SNN and SNB during spring-summer leading to the observed exceedances. Moreover, the change in the wind occurrence in autumn at SNB leads to a lower growth rate than at SNN, where the calmest winds during the whole year drive the largest increase interpreted to be due to the photochemical processing of precursors emitted locally. The GPE and OBI sites exhibit increases only in spring and summer, with the lowest increases of all sites determined at OBI of 0.48 ppb yr⁻¹ in spring, which contrasts with the largest increase at OBI during the same season. However, such increases are consistent with an increase in the occurrence of NE and E air masses at high speeds (>10 km h⁻¹) during spring-summer. STA shows a significant decrease in the maxima daily O₃ 1-h averages of 0.35 ppb yr⁻¹ in winter, which is consistent with an increase in the occurrence of NW air masses at WS < 5 km h⁻¹, loaded with high NO_x mixing ratios (50 ppb) that promote the O₃ titration.

4. Discussion

4.1 Strategies for air quality control in Mexico

The Mexican environmental authorities have focused largely on improving the air quality within the MCMA since 1986, by implementing numerous strategies to control primary emissions, but have paid less attention to other large metropolitan areas in Mexico (PICCA, 1990; ProAire-MCMA, 2011). Control measures have been designed based on NAEI and local emission inventories data, which possess significant uncertainties (Arriaga-Colina et al., 2004; Velasco et al., 2007; Kanda et al., 2016). However, despite these uncertainties, the emission control strategies have helped to reduce O₃ levels within the MCMA since 1991-1992 (ProAire-MCMA, 2001). Here, we describe the most effective measures introduced to control O₃ precursor emissions within the MCMA, and then discuss potential benefits of implementing such measures within the MMA.

From 1993 to 2014, NO_x levels within the MCMA decreased at a rate of around 1.2 ppb yr⁻¹ (1.6 % yr⁻¹) as determined from ground-based measurements. This decline is remarkably consistent with the decrease during 2005-2014 in the NO₂ column over the MCMA of 1.6 % yr⁻¹ reported by Duncan et al.

493 (2016). The decrease in NO_x has been driven largely by reductions in emissions from on-road sources,
494 in response to the introduction of mandatory 3-way catalytic converters in new vehicles since 1993
495 (NOM-042; SEMARNAT, 1993), and by the introduction of a no driving day and more stringent exhaust
496 emissions inspection programs for private cars since 1989 (NOM-041; SEMARNAT, 1993). The NO_x
497 reduction measures also required public transport vehicles to switch from petrol to LP gas fuelled
498 engines, new road corridors were designed for improving the intracity transport and the public transport
499 fleet was renewed (ProAire-MCMA, 2001). For industrial sources, the switch from fuel oil to LP gas fuel,
500 relocation of highly polluting industries away from the MCMA, and implementation of regular inspections
501 programs of NO_x emission for industrial and area sources were also implemented (ProAire-MCMA,
502 2001).

503
504 While the outlook for NO_x levels within the MCMA is clear, studies of VOCs levels have reported no
505 concluding trends. For instance, Arriaga-Colina et al. (2004) reported a decrease in VOCs of around 10
506 % from 1992 to 2001 over the N MCMA, while Garzón et al. (2015) reported that on average VOCs
507 increased over most of the MCMA between 1992-2002 but decreased by 2.4 ppb yr⁻¹ between 2002-
508 2012. However, the decrease in VOCs from 2002 to 2012 reported by Garzón et al. (2015) is consistent
509 with a reduction in light alkanes and aromatics levels during the morning rush hour reported by Jaimes-
510 Palomera et al. (2016). Continuous measurements of VOCs have been introduced recently by the MCMA
511 government, which precludes an assessment of VOCs long-term trends. The measures implemented to
512 control VOCs emissions from on-road sources have included the reformulation of petrol with the
513 reduction of highly reactive VOCs and addition of oxygenated compounds, and fitting of 3-way catalytic
514 converter in all new vehicles (NOM-042; SEMARNAT, 1993; ProAire-MCMA, 2001). For area sources,
515 control measures include the introduction of vapour emissions control systems at petrol stations and
516 introduction of a LP gas leak detection program for the distribution network (ProAire-MCMA, 2011). As
517 for NO_x, industrial VOCs emission sources have been subject to regular emissions inspections and
518 relocation of the most significant emitters (ProAire-MCMA, 2011).

519
520 Therefore, the moderate success on controlling O₃ levels within the MMA can be interpreted as the
521 implementation of effective controls measures on VOCs and NO_x emissions. Thus, a comparison
522 between VOCs and NO_x trends derived from the NAEI and local emissions inventories with those
523 determined from ground-levels measurements can provide insight into further improvements in
524 decreasing O₃ levels not only within the MCMA but also at other large metropolitan areas in Mexico.
525 Within the MCMA, the NAEI NO_x emissions trends are consistent with the decrease determined from
526 ground-based measurements made by SIMAT, but the MCMA local inventory trends disagree with the
527 SIMAT trends (Fig. S1 and Fig. 10). For VOCs, the NAEI and the MCMA inventories oppose measured
528 trends in VOCs during 1993-2001 (Arriaga-Colina et al., 2004; Garzón et al., 2015). This can be
529 explained by underestimates of VOC emissions within the MCMA of a factor of 2-3 (Arriaga-Colina et al.,

2004; Velasco et al., 2007). Such discrepancies suggest that, significant improvements in NO_x and VOCs emissions inventories are still required to better inform O₃ control strategies.

4.2 Ground-level O₃ and O_x variations within the MMA

The O₃ and O_x diurnal variations result from the particular chemical environment and meteorological conditions at each monitoring site within the MMA. Thus, the largest O₃ and O_x mixing ratios, except for OBI, are observed typically for air masses from the E and SE wind sectors, whereas at OBI, the largest O₃ and O_x values are recorded during the occurrence of NE and E air masses. It is clear that short-range transport and large upwind emissions of O₃ precursors from the industrial area dominate the MMA (SEMARNAT, 2006, 2011, 2014; SDS, 2015). This is underlined at OBI with the highest values of O_x where the predominant wind direction is NE, consistent with the transport of emissions from the industrial area located NE, and photochemical processing of air masses (Carrillo-Torres et al., 2017). The daily cycles of O₃ determined within the MMA are consistent with those reported for Los Angeles (VanCuren, 2015), and Toronto (Pugliese et al., 2014). At Toronto, the O₃ maxima were enhanced by the arrival of photochemical processed air masses transported from polluted wind sectors, and decreased during clear air masses. This behaviour is similar to that observed within the MCMA with enhanced O₃ maxima during the occurrence of E-SE (polluted) and decreased levels when SW-W (relatively clean) air masses occurred.

4.3. Origin of the O₃ annual cycles within the MMA

The O₃ annual cycles within the MCMA are consistent with the spring maxima and winter minima characteristic of the US southeast regions (Strode et al., 2015), and follow the O₃ cyclic pattern at NH mid-latitudes (Monks 2000; Vingarzan, 2004). However, they are different to O₃ annual cycles reported for the US west coast regions, particularly in California, where the maxima in the cycle occurs between June-August, driven the local influence of precursor emissions upon O₃ production and photochemical conditions (Vingarzan, 2004; Strode et al., 2015). The recurrent downward spikes in the O₃ annual cycles within the MMA between July-August result from high wind speeds (>10 km h⁻¹ on average) that disperse O₃ precursors and increase the boundary layer height (ProAire-MMA, 2008). The peak in O₃ observed in September is characteristic of humid regions, and can be ascribed to an increase in OH radicals derived from the increment in RH during the rainy season (Lee et al., 2014). A marked increase in RH within the MMA during September is consistent with the increase in O₃ observed as reported by Lee et al. (2014). Over the mid-western and eastern US regions, that O₃ peak has become less noticeable since 2000 (Zheng et al., 2007).

The annual variability in O₃ within the MMA is strongly coupled to the economic conditions (GDP) in Mexico. For instance, the economic crisis of 1994-1996 caused a marked reduction in industrial emissions of VOCs and NO_x, which is confirmed by the significantly decrease in O₃ annual variations at all sites within the MMA (Tiwari et al., 2014; INEGI, 2016). During the global economic recession of 2008-

2009, Castellanos and Boersma (2012) reported a reduction of 10-30 % in tropospheric NO₂ over large European urban areas, which is consistent with a faster decline of $8 \pm 5 \text{ \% yr}^{-1}$ in the NO₂ column density during the same period for US urban regions (Russell et al., 2012). Increases in the NO₂ column density over the MMA as reported by Duncan et al. (2016) are explained by the gradual recovery of the economy since 1997 in Mexico. Moreover, increases in O₃ precursor emissions and in annual variability observed within the MMA are consistent with such economic growth. This explains clearly the opposite trends in O₃ annual variations before and after the economic crisis within the MMA, with the lowest changes seen at the urban GPE site and the greatest ones detected for the SNN industrial site.

4.4 Increasing O₃ and O_x levels within the MMA

Ground-based measurements made during 1993-2014 reveal significant ($p < 0.05$) increases in NO_x within the MMA at all sites, apart from OBI, which exhibits a significant decrease (Fig. 13). Overall, the NO_x increase within the MMA of 1.24 \% yr^{-1} (0.33 ppb yr^{-1}) during 1993-2014 is larger than the increase in the NO₂ column density over the MMA of around 0.78 \% yr^{-1} during 2005-2014 reported by Duncan et al. (2016), although both indicate a significant increase in the NO_x levels at least since 2005. The largest increases in NO_x correspond to industrial sites, SNN (0.51 ppb yr^{-1}) and SNB (0.74 ppb yr^{-1}), which is interpreted as a response to growing industrial activity, in combination with flexible emission regulations within the MMA (INEGI, 2016). The influence of industrial emissions upon O₃ at the MMA becomes evident by the lowest NO_x growth rate observed at GPE of 0.19 ppb yr^{-1} , since OBI has few occurrences of air masses transporting pollutants from the largely industrialised areas throughout the year (Fig. 2). By contrast, the NO_x decrease at OBI of $-0.40 \text{ ppb yr}^{-1}$ arises from decreases in emissions from on-road sources (SDS, 2015). The large growth rates in O₃ and NO_x at SNN and SNB are explained by increasing emissions of O₃ precursors from a growing number of industries and the urban development E of the MMA. The most likely explanation for the O₃ increase at OBI is a reduced titration effect by decreasing NO_x levels in combination with the non-linear response in O₃ production to decreasing NO_x emissions under the VOC-sensitive MMA airshed (Sierra et al., 2013; Menchaca-Torre et al. 2015).

The O_x long-term trends during 1993-2014 within the MMA were consistent with those for O₃ at all sites. Decreases in NO_x and O₃ observed between 1994-1996 were the response to the economic crisis during the same period in Mexico, when the DGP decreased by 5.9 % providing additional evidence of the dominant role of industries within the MMA. Consistent with economic indicators, annual averaged petrol sales in the Nuevo Leon state in 1995 decreased by 2.4 % in relation to 1994, but increased linearly from 1996 to 2008 at an approximate rate of $98,800 \text{ m}^3 \text{ petrol yr}^{-1}$ ($r = 0.90$) (Fig. S11) (SENER, 2015). As for petrol sales, registered vehicles in Nuevo Leon show significant variations between 1993-1996, but increase linearly since 1997 at a rate of around $100,000 \text{ vehicles yr}^{-1}$ ($r=0.99$). This confirms that despite the annual growth in the vehicular fleet, the fitting of 3-way catalyst technology and reformulation of petrol introduced in 1997 has controlled on-road primary emissions (ProAire-MCMA, 2001) The decreases in NO_x observed at OBI and at all sites during the occurrence of SW-W-NW air masses reflect that if

606 applied, stricter emissions controls such as those for on-road sources can lead to a significant abatement
607 in primary emissions. It is clear that the industrial sources must be subject to similar emission control
608 measures as those implemented within the MMA for effectively reducing the O₃ levels.

610 **4.5 The opposite O₃ trends at Mexican urban areas**

611 The comparison of O₃ and O_x trends at MMA, GMA and MCMA reveals different emission trends at each
612 of the studied cities. The trends in O₃ reported in this study for the MCMA, agree with the reduction of
613 20 ppb O₃ during 1991-2011 for the MCMA (Jaimes et al., 2012), and with the reduction of 8 ppb O₃
614 during 2000-2011 for the MMA (Benítez-García et al., 2014). At the GMA, the no trend status in O₃
615 determined here is in contrast with the increase of 12 ppb O₃ during 2000-2011 (Benítez-García et al.,
616 2014), which is due to the different periods assessed in the latter. Decreases in O₃ in US urban areas
617 arise from effective control of O₃ precursor emissions (Strode et al., 2015), which has occurred at the
618 MCMA.

620 Figure 10 shows that NO_x decreased significantly within the MCMA (1.57 % yr⁻¹) and the GMA (1.83 %
621 yr⁻¹) during 1993-2014 and 1996-2014, respectively, but increased within the MMA (1.83 % yr⁻¹) during
622 1993-2014. Such NO_x trends are within the range of the trends in the NO₂ column density reported by
623 Duncan et al. (2016) in Table S9, which reveals an increase of 0.78 ± 1.12 % yr⁻¹ for the MMA, but
624 decreases of 1.82 ± 0.84 % yr⁻¹ for the GMA and of 0.10 ± 1.67 % yr⁻¹ for the MCMA, all during 2005-
625 2014. To date, long-term trends in VOCs have only been reported only the MCMA with an average
626 decrease of ca. 2.4 ppb yr⁻¹ since 2002, mostly in propane, ethanol and acetone (Garzón et al., 2016),
627 while there are no studies of long-term trends in VOCs within the MMA and the GMA.

629 It has been shown that O₃ and O_x decreases within the MCMA have been driven by reductions in NO_x
630 and VOCs emissions, and that the implemented strategies described in Sect. 4.1 have proved to be
631 effective in controlling primary emissions (ProAire-MCMA, 2011; Jaimes-Palomera et al., 2016). By
632 contrast, growing industrial emissions within the MMA must be subject to stringent controls to abate O₃
633 levels. In the GMA, where the industrial activity is lower than at the MCMA and MMA (Kanda et al., 2016),
634 the policies introduced at national scale for controlling on-road sources emissions have resulted in the
635 decrease of NO_x emissions and in the stabilisation of O₃ levels. The results presented here demonstrate
636 the merits of the assessment and analysis of long-term O₃ levels, which can be used by environmental
637 authorities to revise and to redesign programs and policies to improve air quality. Continuing with ground-
638 based O₃ and NO_x monitoring is strongly recommended to better understand the response further
639 changes in local and regional O₃ levels to changes in primary emissions. Monitoring of VOCs at the GMA
640 and MMA is also recommended to as the VOCs emissions data reported in the NAEI possess significant
641 uncertainties. Finally, according to the results presented here, we recommend preferentially reducing
642 VOCs emissions, which may limit O₃ production in response to a decrease in the VOCs/NO_x ratio.
643 However, simultaneously reducing NO_x will have added health benefits of less NO₂.

644

645 **5. Conclusions**

646 Diurnal and annual cycles, and long-term trends in O_3 and O_x within the MMA, are interpreted as
 647 response to changes in NO_x and VOCs emissions, photochemistry and meteorology. Continuous high-
 648 frequency and high-precision O_3 and NO_x data recorded during 1993-2014 at 5 sites within the MMA
 649 and at 29 sites within the MCMA, and during 1996-2014 at 10 sites within the GMA, were used to
 650 calculate long-term trends. Within the MMA, the greatest mixing ratios in O_3 were recorded during E and
 651 SE winds, at sites downwind of significant precursors from industrial sources. By contrast, the lowest O_3
 652 mixing ratios were recorded at SNN, and for all sites were observed for the W and SW sectors, where
 653 air masses travel from central Mexico over 100-300 km of semi-arid region sparsely populated. Maximum
 654 daily 1-h values of O_3 and O_x increased significantly at GPE, SNN and SNB, owing to increasing
 655 emissions of precursors, while at OBI increasing O_3 and decreasing O_x trends arise from the non-linear
 656 response to decreasing NO_x emissions from on-road sources.

657

658 Annual cycles in O_3 at all sites peak in spring and through in winter, with a downward spike during
 659 summer caused by high winds that disperse O_3 , and increase the boundary layer height. Decreases in
 660 O_3 precursor emissions during the economic crisis experienced in Mexico between 1994-1996, caused
 661 significant decline trends O_3 annual variations from 1993 to 1997 or 1998, depending on site, followed
 662 by significant increases derived from the recovery of the economy. The dominant role of industrial
 663 sources on O_3 precursor levels within the MMA was evident at the industrial site SNN during the 1994-
 664 1996 economic crisis.

665

666 At all metropolitan areas studied, O_3 and O_x levels showed no significant differences between weekdays
 667 and weekend, although an earlier occurrence of the O_3 peak at the GMA was detected, ascribed to larger
 668 VOCs/ NO_x emission ratio. The lack of the weekend effect was attributed to weekday O_3 production being
 669 limited by VOCs, whereas increases in the VOC/ NO_x ratio during weekends in response to reduced
 670 emissions from mobile sources resulted in similar O_3 mixing ratios that during weekdays. Larger AV_{δ} s
 671 during weekdays and weekends were seen at MCMA than at GMA and MMA related to the relative
 672 emissions of the O_3 precursors.

673

674 Significant seasonal trends in O_3 and O_x during spring were observed at all sites, apart from STA,
 675 whereas industrial sites exhibited significant increases for O_x in all seasons. The largest increases in O_3
 676 and O_x were observed during the occurrence of NE-E-SE air masses. The only significant decrease in
 677 O_x at STA was related to the NW wind occurrence during winter. NO_x mixing ratios increased significantly
 678 at all sites, except at OBI, due to the dominant role of industrial sources on NO_x levels. The overall
 679 significant increasing trend of $0.22 \text{ ppb } O_3 \text{ yr}^{-1}$ within the MMA contrasts within a significant decreasing
 680 trend of $1.15 \text{ ppb } O_3 \text{ yr}^{-1}$ within the MCMA during 1993-2014, whereas a non-significant trend is evident
 681 within the GMA during 1996-2014. At the MCMA and GMA, the overall O_x trends reflect the trends in O_3

precursors. According to the long-term trends in O₃ for the MMA, the number of exceedances of the air quality standards will very likely increase as result of increasing precursor emissions. The moderate mitigation of O₃ levels within the MCMA, derived from measures implemented to control emissions from on-road, industrial and area sources, emphasises the need for more stringent control of emissions mostly from industrial sources within the MMA in order to improve air quality. Finally, comparison between emission inventories estimates of NO_x and VOCs with ground-based measurements, indicate that significant reductions in uncertainties are required to better inform air quality policies.

6. Acknowledgments

This research was supported by Tecnológico de Monterrey through the Research Group for Energy and Climate Change (Grant 0824A0104 and 002EICIR01). Grateful acknowledgements are made to the Secretariat for Sustainable Development of the Nuevo Leon State, the Secretariat for the Environment of Mexico City and the Secretariat for the Environment and Territorial Development of the Jalisco State for the public domain records. We gratefully thank the NOAA Air Resources Laboratory (ARL) for access to the HYSPLIT model and READY website (<http://www.ready.noaa.gov>), and Dr. Sigfrido Iglesias for providing the imputed O₃ and NO_x data for the MMA time-series. We are also grateful to Professor Paul Monks and Professor Richard Derwent for encouraging comments on an earlier version of the manuscript.

7. References

- Akimoto, H., Mori, Y., Sasaki, K., Nakanishi, H., Ohizumi, T., and Itano, Y.: Analysis of monitoring data of ground-level ozone in Japan for long-term trend during 1990-2010: Causes of temporal and spatial variation, *Atmos. Environ.*, 102, 302-310, doi:10.1016/j.atmosenv.2014.12.001, 2015.
- Arriaga-Colina, J. L., West, J. J., Sosa, G., Escalona, S. S., Ordunez, R. M., and Cervantes, A. D. M. Measurements of VOCs in Mexico City (1992–2001) and evaluation of VOCs and CO in the emissions inventory, *Atmos. Environ.*, 38, 2523-2533, doi:10.1016/j.atmosenv.2004.01.033, 2004.
- Atkinson, R.: Atmospheric chemistry of VOCs and NO_x. *Atmos. Environ.*, 34, 2063-2101, doi:10.1016/S1352-2310(99)00460-4, 2000.
- Benítez-García, S. E., Kanda, I., Wakamatsu, S., Okazaki, Y., and Kawano, M.: Analysis of criteria air pollutant trends in three Mexican metropolitan areas, *Atmosphere*, 5, 806-829, doi:10.3390/atmos5040806, 2014.
- Boersma, K. F., Jacob, D. J., Bucsela, E. J., Perring, A. E., Dirksen, R., van der A, R. J., Yantosca, R. M., Park, R. J., Wenig, M. O., Bertram, T. H., and Cohen, R. C.: Validation of OMI tropospheric NO₂ observations during INTEx-B and application to constrain NO_x emissions over the eastern United States and Mexico, *Atmos. Environ.*, 42, 4480-4497. doi:10.1016/j.atmosenv.2008.02.004, 2008.
- Butler, T. M., Stock, Z. S., Russo, M. R., Denier Van Der Gon, H. A. C., and Lawrence, M. G.: Megacity ozone air quality under four alternative future scenarios, *Atmos. Chem. Phys.*, 12, 4413-4428, doi:10.5194/acp-12-4413-2012, 2012.
- Camalier, L., Cox, W., and Dolwick, P.: The effects of meteorology on ozone in urban areas and their use in assessing ozone trends, *Atmos. Environ.*, 41, 7127-7137, doi: 10.1016/j.atmosenv.2007.04.061, 2007.

723 Carrillo-Torres, E. R., Hernández-Paniagua, I. Y., and Mendoza, A.: Use of combined observational-and
 724 model-derived photochemical indicators to assess the O₃-NO_x-VOC system sensitivity in urban areas,
 725 *Atmosphere*, 8, 22, doi:10.3390/atmos8020022, 2017.

726 Carslaw, D. C., and Ropkins, K.: openair - An R package for air quality data analysis, *Environ. Model.*
 727 *Soft.*, 27-28, 52-61, doi:10.1016/j.envsoft.2011.09.008, 2012.

728 Carslaw, D. C.: The openair manual - open-source tools for analysing air pollution data, Manual for
 729 version 1.1-4, King's College London, 2015.

730 Castellanos, P. and Boersma, K. F.: Reductions in nitrogen oxides over Europe driven by environmental
 731 policy and economic recession, *Sci. Rep.*, 2, doi:10.1038/srep00265, 2012.

732 Clapp, L. J., and Jenkin, M. E.: Analysis of the relationship between ambient levels of O₃, NO₂ and NO
 733 as a function of NO_x in the UK. *Atmospheric Environment*, 35, 6391-6405, doi: 10.1016/S1352-
 734 2310(01)00378-8, 2001.

735 Cleveland, R. B., Cleveland, W. S., McRae, J., and Terpenning, I.: STL: A seasonal-trend decomposition
 736 procedure based on Loess, *J. Off. Stats.*, 6, 3-33, 1990.

737 Dentener, F., Stevenson, D., Cofala, J., Mechler, R., Amann, M., Bergamaschi, P., Raes, F., and
 738 Derwent, R.: The impact of air pollutant and methane emission controls on tropospheric ozone and
 739 radiative forcing: CTM calculations for the period 1990-2030, *Atmos. Chem. Phys.*, 5, 1731-1755,
 740 doi:10.5194/acp-5-1731-2005, 2005.

741 Duncan, B. N., Lamsal, L. N., Thompson, A. M., Yoshida, Y., Lu, Z., Streets, D. G., Hurwitz, M. M., and
 742 Pickering, K. E.: A space-based, high-resolution view of notable changes in urban NO_x pollution around
 743 the world (2005–2014), *J. Geophys. Res.*, 121, 976–996, doi:10.1002/2015JD024121, 2016.

744 Durbin, J., and Koopman, S. J.: Time Series Analysis by State Space Methods, Oxford University Press,
 745 Oxford UK, 2nd Edition, 2012.

746 EPA (Environmental Protection Agency US): Compilation of Air Pollution Emission Factors (AP-42),
 747 Volume I: Stationary Point and Area Sources, available at: [https://www.epa.gov/air-emissions-factors-](https://www.epa.gov/air-emissions-factors-and-quantification/ap-42-compilation-air-emission-factors)
 748 [and-quantification/ap-42-compilation-air-emission-factors](https://www.epa.gov/air-emissions-factors-and-quantification/ap-42-compilation-air-emission-factors), last access: 14 Jan 2017, 1995.

749 EPA (Environmental Protection Agency US): User's Guide to MOBILE6.1 and MOBILE6.2: Mobile
 750 Source Emission Factor Model, available at: [https://www3.epa.gov/otaq/models/mobile6/](https://www3.epa.gov/otaq/models/mobile6/420r03010.pdf)
 751 [420r03010.pdf](https://www3.epa.gov/otaq/models/mobile6/420r03010.pdf), last access: 16 Jan 2017, 2003.

752 EPA (Environmental Protection Agency US): Air quality trends, available at: [https://www.epa.gov/air-](https://www.epa.gov/air-trends)
 753 [trends](https://www.epa.gov/air-trends), last access: 15 Jan 2017, 2009.

754 Garzón, J. P., Huertas, J. I., Magaña, M., Huertas, M. E., Cárdenas, B., Watanabe, T., Maeda, T.,
 755 Wakamatsu, S., and Blanco, S.: Volatile organic compounds in the atmosphere of Mexico City, *Atmos.*
 756 *Environ.*, 119, 415-429, doi:10.1016/j.atmosenv.2015.08.014, 2015.

757 Guicherit, R., and Roemer, M.: Tropospheric ozone trends, *Chemosphere*, 2, 167-183,
 758 doi:10.1016/S1465-9972(00)00008-8, 2000.

759 Hernández-Paniagua, I. Y., Lowry, D., Clemitshaw, K. C., Fisher, R. E., France, J. L., Lanoisellé, M.,
 760 Ramonet, M., and Nisbet, E. G.: Diurnal, seasonal, and annual trends in atmospheric CO₂ at southwest
 761 London during 2000-2012: Wind sector analysis and comparison with Mace Head, Ireland, *Atmos.*
 762 *Environ.*, 105, 138-147, doi: 10.1016/j.atmosenv.2015.01.02, 2015.

763 INE (Instituto Nacional de Ecología): Cuarto almanaque de datos y tendencias de la calidad del aire en
 764 20 ciudades Mexicanas 2000-2009, INE-SEMARNAT, México, D.F., 405 pp., 2011.

765 INEGI (National Institute of Statistics and Geography): XIII Censo General de Población y Vivienda 2010,
 766 México, available at: <http://www.censo2010.org.mx/>, last Access: 22 May 2016, 2010.

767 INEGI (National Institute of Statistics and Geography): México en Cifras, México, available at:
 768 <http://www3.inegi.org.mx/sistemas/mexicocifras/default.aspx?e=19>, last access: 22 May 2016, 2015.

769 INEGI (National Institute of Statistics and Geography): Producto Interno Bruto (GDP)–Trimestral 2016,
 770 available at: <http://www.inegi.org.mx/est/contenidos/proyectos/cn/pibt/>, last access: 11 Jan 2017, 2016.

771 IPCC: Climate Change 2013: The Physical Science Basis. Contribution of Working Group I to the Fifth
 772 Assessment Report of the Intergovernmental Panel on Climate Change, 2013. [Stocker, T.F., D. Qin, G.-
 773 K. Plattner, M. Tignor, S.K. Allen, J. Boschung, A. Nauels, Y. Xia, V. Bex and P.M. Midgley (eds.)].
 774 Cambridge University Press, Cambridge, United Kingdom and New York, NY, USA, 1535 pp., 2013.

775 Jaimes, P. M., Bravo, A. H., Sosa, E. R., Cureño, G. I., Retama, H. A., Granados, G. G., and Becerra,
 776 A. E.: Surface ozone concentration trends in Mexico City Metropolitan Area, in: Proceedings of the Air
 777 and Waste Management Association's Annual Conference and Exhibition AWMA, San Antonio, Texas,
 778 19-22 June 2012, 3, 2273-2284, 2012.

779 Jaimes-Palomera, M., Retama, A., Elias-Castro, G., Neria-Hernández, A., Rivera-Hernández, O., and
 780 Velasco, E.: Non-methane hydrocarbons in the atmosphere of Mexico City: Results of the 2012 ozone-
 781 season campaign, *Atmos. Environ.*, 132, 258-275, doi:10.1016/j.atmosenv.2016.02.047, 2016.

782 Jenkin, M. E., and Clemitshaw, K. C.: Ozone and other secondary photochemical pollutants: chemical
 783 processes governing their formation in the planetary boundary layer, *Atmos. Environ.*, 34(16), 2499-
 784 2527, doi:10.1016/S1352-2310(99)00478-1, 2000.

785 Kanda, I., Basaldud, R., Magaña, M., Retama, A., Kubo, R., and Wakamatsu, S.: Comparison of Ozone
 786 Production Regimes between Two Mexican Cities: Guadalajara and Mexico City, *Atmosphere*, 7, 91,
 787 doi:10.3390/atmos7070091, 2016.

788 Lee, Y. C., Shindell, D. T., Faluvegi, G., Wenig, M., Lam, Y. F., Ning, Z., Hao, S., and Lai, C. S.: Increase
 789 of ozone concentrations, its temperature sensitivity and the precursor factor in South China, *Tellus B*.
 790 *Chem. Phys. Meteorol.*, 66, doi:10.3402/tellusb.v66.23455, 2014.

791 Lefohn, A. S., Shadwick, D., and Oltmans, S. J.: Characterizing changes in surface ozone levels in
 792 metropolitan and rural areas in the United States for 1980-2008 and 1994-2008, *Atmos. Environ.*, 44,
 793 5199–5210, doi: 10.1016/j.atmosenv.2010.08.049, 2010.

794 Lei, W., de Foy, B., Zavala, M., Volkamer, R., and Molina, L. T.: Characterizing ozone production in the
 795 Mexico City Metropolitan Area: a case study using a chemical transport model, *Atmos. Chem. Phys.*, 7,
 796 1347-1366, doi:10.5194/acp-7-1347-2007, 2007.

797 Lelieveld, J., Evans, J. S., Fnais, M., Giannadaki, D., and Pozzer, A.: The contribution of outdoor air
 798 pollution sources to premature mortality on a global scale, *Nature Letts.*, 15371,
 799 doi:10.1038/nature15371, 2015.

800 Menchaca-Torre, H. L., Mercado-Hernández, R., and Mendoza-Domínguez, A.: Diurnal and seasonal
 801 variation of volatile organic compounds in the atmosphere of Monterrey, Mexico, *Atmos. Poll. Res.*, 6,
 802 1073-1081, doi:10.1016/j.apr.2015.06.004, 2015.

803 Molina, M. J., and Molina, L. T.: Megacities and atmospheric pollution, *J. Air Waste Manage.*, 54, 644-
 804 680, doi:10.1080/10473289.2004.10470936, 2004.

805 Monks, P. S.: A review of the observations and origins of the spring ozone maximum, *Atmos. Environ.*,
 806 34, 3545-3561, doi:10.1016/S1352-2310(00)00129-1, 2000.

807 Monks, P. S., Archibald, A. T., Colette, A., Cooper, O., Coyle, M., Derwent, R., Fowler, D., Granier, C.,
 808 Law, K. S., Mills, G. E., Stevenson, D. S., Tarasova, O., Thouret, V., von Schneidmesser, E.,
 809 Sommariva, R., Wild, O., and Williams, M. L.: Tropospheric ozone and its precursors from the urban to
 810 the global scale from air quality to short-lived climate forcer, *Atmos. Chem. Phys.*, 15, 8889-8973,
 811 doi:10.5194/acp-15-8889-2015, 2015.

812 Parrish, D. D., Millet, D. B., and Goldstein, A. H.: Increasing ozone in marine boundary layer inflow at
813 the west coasts of North America and Europe, *Atmos. Chem. Phys.*, 9, 1303-1323, doi:10.5194/acp-9-
814 1303-2009, 2009.

815 Parrish, D. D., Singh, H. B., Molina, L., and Madronich, S.: Air quality progress in North American
816 megacities: A review, *Atmos. Environ.*, 45, 7015-7025, doi:10.1016/j.atmosenv.2011.09.039, 2011.

817 PICCA (Programa integral contra la contaminación atmosférica de la zona metropolitana de la Ciudad
818 de México), Mexico City Local Government, available at: [http://centro.paot.org.mx/documentos/
819 varios/prog_inte_atmosferica.pdf](http://centro.paot.org.mx/documentos/varios/prog_inte_atmosferica.pdf), last Access: 28 April 2017, 1990

820 ProAire-MMA (Programa de Gestión para Mejorar la Calidad del Aire del Área Metropolitana de
821 Monterrey 2008-2012), SEMARNAT, Gobierno del estado de Nuevo León, available at:
822 [http://www.semarnat.gob.mx/archivosanteriores/temas/gestionambiental/calidaddelaire/
823 Documents/Calidad%20del%20aire/Proaires/ProAires_Vigentes/6_ProAire%20AMM%202008-
824 2012.pdf](http://www.semarnat.gob.mx/archivosanteriores/temas/gestionambiental/calidaddelaire/Documents/Calidad%20del%20aire/Proaires/ProAires_Vigentes/6_ProAire%20AMM%202008-2012.pdf), last access: 22 May 2016, 2008.

825 ProAire-MCMA (Programa para Mejorar la Calidad del Aire de la Zona Metropolitana del Valle de México
826 2002-2010), Mexico City Local Government-State of Mexico Government, available at:
827 http://www.gob.mx/cms/uploads/attachment/file/69312/11_ProAire_ZMVM_2002-2010.pdf, last access:
828 28 April, 2017, 2001.

829 ProAire-MCMA (Programa para Mejorar la Calidad del Aire de la Zona Metropolitana del Valle de México
830 2002-2010), Mexico City Local Government-State of Mexico Government, available at:
831 <http://www.aire.cdmx.gob.mx/descargas/publicaciones/flippingbook/proaire2011-2020/#p=1>,
832 last access: 28 April 2017, 2011

833 Pugliese, S. C., Murphy, J. G., Geddes, J. A., and Wang, J. M.: The impacts of precursor reduction and
834 meteorology on ground-level ozone in the Greater Toronto Area, *Atmos. Chem. Phys.*, 14, 8197-8207,
835 doi:10.5194/acp-14-8197-2014, 2014.

836 Pusede, S. E., and Cohen, R. C. On the observed response of ozone to NO_x and VOC reactivity
837 reductions in San Joaquin Valley California 1995–present, *Atmos. Chem. Phys.*, 12, 8323-8339,
838 doi:10.5194/acp-12-8323-2012, 2012.

839 Pusede, S. E., Steiner, A. L., and Cohen, R.C.: Temperature and recent trends in the chemistry of
840 continental surface ozone, *Chem. Rev.*, 115, 3898-3918, doi: 10.1021/cr5006815, 2015.

841 R Core Team: R: a Language and Environment for Statistical Computing, R Foundation for Statistical
842 Computing, Vienna, Austria, ISBN 3-900051-07-0, 2013, available at: www.R-project.org, last access:
843 23 May 2016, 2013.

844 Radian (International): Mexico Emissions Inventory Program Manuals (Vol. II-VI), available at:
845 https://www3.epa.gov/ttnecat1/cica/other3_s.html, last access: 15 Jan 2017, 2000.

846 Reinsel, G. C.: Elements of Multivariate Time Series Analysis. Springer-Verlag, New York, USA, 2nd
847 Edition, 1997.

848 Revell, L. E., Tummon, F., Stenke, A., Sukhodolov, T., Coulon, A., Rozanov, E., Garny, H., Grewe, V.
849 and Peter, T.: Drivers of the tropospheric ozone budget throughout the 21st century under the medium-
850 high climate scenario RCP 6.0, *Atmos. Chem. Phys.*, 15, 5887-5902, doi:10.5194/acp-15-5887-2015,
851 2015.

852 Rodríguez, S., Huerta, G., and Reyes, H.: A study of trends for Mexico City ozone extremes: 2001-2014,
853 *Atmosfera*, 29, 107-120, doi:10.20937/ATM.2016.29.02.01, 2016.

854 Russell, A. R., Valin, L. C., and Cohen, R. C.: Trends in OMI NO₂ observations over the United States:
855 effects of emission control technology and the economic recession, *Atmos. Chem. Phys.*, 12, 12197-
856 12209, doi:10.5194/acp-12-12197-2012, 2012.

857 Salmi, T., Määttä, A., Anttila, P., Ruoho-Airola, T. and Amnell, T.: Detecting trends of annual values of
858 atmospheric pollutants by the Mann-Kendall test and Sen's slope estimates – the Excel template
859 application MAKESENS, Publications on Air Quality Report code FMI-AQ-31, Helsinki, Finland, 31, 1-
860 35, 2002.

861 Schultz, M., and Rast, S.: REanalysis of the TROpospheric chemical composition over the past 40 years,
862 Emission Data Sets and Methodologies for Estimating Emissions, Work Package 1, Deliverable D1-6,
863 available at: http://retro-archive.iek.fz-juelich.de/data/documents/reports/D1-6_final.pdf, last access: 14
864 Jul 2016, 2007.

865 SDS (Secretaria de Desarrollo Sustentable), Inventario de emisiones del Área Metropolitana de
866 Monterrey 2013, personal communication, Monterrey, N.L. México, 4 Sep 2015.

867 SDS (Secretaria de Desarrollo Sustentable): Sistema Integral de Monitoreo Ambiental, available at:
868 <http://aire.nl.gob.mx/>, last access: 21 May 2016, 2016.

869 SEDEMA (Secretaria del Medio Ambiente): INVENTARIO de Emisiones a la Atmosfera en la ZMVM
870 1996, available at: <http://www.sedema.df.gob.mx/flippingbook/inventario-emisiones-1996/#p=1>, last
871 access: 20 May 2016, 1999.

872 SEDEMA (Secretaria del Medio Ambiente): Inventario de Emisiones Zona Metropolitana del Valle de
873 Mexico 1998, available at: [http://www.sedema.df.gob.mx/flippingbook/inventario-emisiones-](http://www.sedema.df.gob.mx/flippingbook/inventario-emisiones-zmvm1998/#p=75)
874 [zmvm1998/#p=75](http://www.sedema.df.gob.mx/flippingbook/inventario-emisiones-zmvm1998/#p=75), last access: 20 May 2016, 2001.

875 SEDEMA (Secretaria del Medio Ambiente): Inventario de emisiones a la Atmosfera Zona Metropolitana
876 del Valle de Mexico 2000, available at: [http://www.sedema.df.gob.mx/](http://www.sedema.df.gob.mx/flippingbook/inventario-emisiones-zmvm2000/) [flippingbook/inventario-](http://www.sedema.df.gob.mx/flippingbook/inventario-emisiones-zmvm2000/)
877 [emisiones-zmvm2000/](http://www.sedema.df.gob.mx/flippingbook/inventario-emisiones-zmvm2000/), last access: 20 May 2016, 2003.

878 SEDEMA (Secretaria del Medio Ambiente): Inventario de emisiones de la Zona Metropolitana del Valle
879 de Mexico 2002, available at: [http://www.sedema.df.gob.mx/flippingbook/inventario-emisiones-zmvm-](http://www.sedema.df.gob.mx/flippingbook/inventario-emisiones-zmvm-criterio2004/#p=1)
880 [criterio2004/#p=1](http://www.sedema.df.gob.mx/flippingbook/inventario-emisiones-zmvm-criterio2004/#p=1), last access: 20 May 2016, 2004.

881 SEDEMA (Secretaria del Medio Ambiente): Inventario de Emisiones Zona Metropolitana del Valle de
882 Mexico 2004, available at: [http://www.sedema.df.gob.mx/flippingbook/inventario-emisiones-zmvm-](http://www.sedema.df.gob.mx/flippingbook/inventario-emisiones-zmvm-criterio2004/#p=1)
883 [criterio2004/#p=1](http://www.sedema.df.gob.mx/flippingbook/inventario-emisiones-zmvm-criterio2004/#p=1), last access: 20 May 2016, 2006.

884 SEDEMA (Secretaria del Medio Ambiente): Inventario de Emisiones de Contaminantes Criterio 2006,
885 available at: <http://www.sedema.df.gob.mx/flippingbook/inventario-emisiones-zmvm-criterio2006/#p=1>,
886 last access: 20 May 2016, 2008.

887 SEDEMA (Secretaria del Medio Ambiente): Inventario de emisiones de contaminantes criterio de la
888 ZMVM 2008, available at: [http://www.sedema.df.gob.mx/flippingbook/inventario-emisiones-zmvm-](http://www.sedema.df.gob.mx/flippingbook/inventario-emisiones-zmvm-criterio2008/#p=1)
889 [criterio2008/#p=1](http://www.sedema.df.gob.mx/flippingbook/inventario-emisiones-zmvm-criterio2008/#p=1), last access: 20 May 2016, 2010.

890 SEDEMA (Secretaria del Medio Ambiente): Inventario de emisiones de la Zona Metroplitiana del Valle
891 de Mexico contaminantes criterio 2010, available at:
892 <http://www.sedema.df.gob.mx/flippingbook/inventario-em1isiones-zmvm-criterio-2010/#p=6>, last
893 access: 20 May 2016, 2012.

894 SEDEMA (Secretaria del Medio Ambiente): Inventario de Emisiones Contaminantes y de efecto
895 invernadero, available at: <http://www.sedema.df.gob.mx/flippingbook/inventario-emisioneszmvm2012/>,
896 last access: 20 May 2016, 2014.

897 SEDEMA (Secretaria del Medio Ambiente de la Ciudad de Mexico): Sistema de Monitoreo Atmosférico,
898 available at: <http://www.aire.df.gob.mx/default.php>, last access: 21 May 2016, 2016a.

899 SEDEMA (Secretaria del Medio Ambiente de la Ciudad de Mexico): Inventario de Emisiones de la CDMX
900 2014 Contaminantes Criterio Tóxicos y de Efecto Invernadero, available at:
901 <http://www.aire.cdmx.gob.mx/descargas/publicaciones/flippingbook/inventario-emisiones-cdmx2014-2/>,
902 last Access: 10 Jan 2017, 2016b.

903 SEMARNAT (Secretaria del Medio Ambiente y Recursos Naturales): NOM-041 (NORMA OFICIAL
904 MEXICANA, QUE ESTABLECE LOS LIMITES MAXIMOS PERMISIBLES DE EMISION DE GASES
905 CONTAMINANTES PROVENIENTES DEL ESCAPE DE LOS VEHICULOS AUTOMOTORES EN
906 CIRCULACION QUE USAN GASOLINA COMO COMBUSTIBLE), Diario Oficial de la Federación, 1993.

907 SEMARNAT (Secretaria del Medio Ambiente y Recursos Naturales): NOM-042 (NORMA OFICIAL
908 MEXICANA QUE ESTABLECE LOS LIMITES MAXIMOS PERMISIBLES DE EMISION DE
909 HIDROCARBUROS TOTALES O NO METANO, MONOXIDO DE CARBONO, OXIDOS DE
910 NITROGENO Y PARTICULAS PROVENIENTES DEL ESCAPE DE LOS VEHICULOS
911 AUTOMOTORES NUEVOS CUYO PESO BRUTO VEHICULAR NO EXCEDA LOS 3,857
912 KILOGRAMOS, QUE USAN GASOLINA, GAS LICUADO DE PETROLEO, GAS NATURAL Y DIESEL,
913 ASI COMO DE LAS EMISIONES DE HIDROCARBUROS EVAPORATIVOS PROVENIENTES DEL
914 SISTEMA DE COMBUSTIBLE DE DICHOS VEHICULOS), Diario Oficial de la Federación, 1993.

915 SEMARNAT (Secretaria del Medio Ambiente y Recursos Naturales): Inventario Nacional de Emisiones
916 1999, México, D.F., available at: <http://www.inecc.gob.mx/dica/548-calaire-inem-1999>, last access: 20
917 May 2016, 2006.

918 SEMARNAT (Secretaria del Medio Ambiente y Recursos Naturales): Inventario Nacional de Emisiones
919 2005, México, D.F., available at: [http://sinea.semarnat.gob.mx/sinae.php?process=](http://sinea.semarnat.gob.mx/sinae.php?process=UkVQT1JURUFET1I=&categ=1)
920 [UkVQT1JURUFET1I=&categ=1](http://sinea.semarnat.gob.mx/sinae.php?process=UkVQT1JURUFET1I=&categ=1), last access: 22 May 2016, 2011.

921 SEMARNAT (Secretaria del Medio Ambiente y Recursos Naturales): Inventario Nacional de Emisiones
922 2008, México, D.F., available at: [http://sinea.semarnat.gob.mx/sinae.php?process=](http://sinea.semarnat.gob.mx/sinae.php?process=UkVQT1JURUFET1I=&categ=14)
923 [UkVQT1JURUFET1I=&categ=14](http://sinea.semarnat.gob.mx/sinae.php?process=UkVQT1JURUFET1I=&categ=14), last access: 22 May 2016, 2014.

924 SEMARNAT (Secretaria del Medio Ambiente y Recursos Naturales): Informe Nacional de calidad del
925 aire 2014, México, D.F., available at: [http://inecc.gob.mx/descargas/calaire/](http://inecc.gob.mx/descargas/calaire/2015_Informe_nacional_calidad_aire_2014_Final.pdf)
926 [2015_Informe_nacional_calidad_aire_2014_Final.pdf](http://inecc.gob.mx/descargas/calaire/2015_Informe_nacional_calidad_aire_2014_Final.pdf), last access: 15 Dec 2016, 2015.

927 SENER (Secretaria de Energia): Estadísticas Energéticas Nacionales, México, available at:
928 <http://sie.energia.gob.mx/bdiController.do?action=temas>, last access: 4 November 2015, 2015.

929 Sicard, P., Serra, R., and Rossello, P.: Spatiotemporal trends in ground-level ozone concentrations and
930 metrics in France over the time period 1999-2012, *Environ. Res.*, 149, 122-144,
931 doi:10.1016/j.envres.2016.05.014, 2016

932 Sierra, A., Vanoye, A. Y., and Mendoza, A.: Ozone sensitivity to its precursor emissions in northeastern
933 Mexico for a summer air pollution episode, *J. Air Waste Manage.*, 63, 1221-1233,
934 doi:10.1080/10962247.2013.813875, 2013.

935 Simon, H., Reff, A., Wells, B., Xing, J., and Frank, N.: Ozone trends across the United States over a
936 period of decreasing NO_x and VOC emissions, *Environ. Sci. Tech.*, 49, 186-195. doi:10.1021/es504514z,
937 2015.

938 SMN (Servicio Meteorológico Nacional), available at: <http://smn.cna.gob.mx/es/>, last access: 21 May
939 2016.

940 Staehelin, J., and Schmid, W.: Trend analysis of tropospheric ozone concentrations utilizing the 20-year
941 data set of ozone balloon soundings over Payerne (Switzerland), *Atmos. Environ.*, 25, 1739-1749,
942 doi:10.1016/0960-1686(91)90258-9, 1991.

943 Stein, A. F., Draxler, R. R., Rolph, G. D., Stunder, B. J. B., Cohen, M. D., and Ngan, F.: NOAA'S HYSPLIT
944 atmospheric transport and dispersion modelling system. *Am. Meteorol. Soc.*, 96, 2059-2077,
945 doi:10.1175/BAMS-D-14-00110.1, 2015.

946 Stephens, S., Madronich, S., Wu, F., Olson, J. B., Ramos, R., Retama, A., and Muñoz, R.: Weekly
947 patterns of México City's surface concentrations of CO, NO_x, PM₁₀ and O₃ during 1986-2007, *Atmos.*
948 *Chem. Phys.*, 8, 5313-5325, doi:10.5194/acp-8-5313-2008, 2008.

949 Stevenson, D. S., Dentener, F. J., Schultz, M. G., Ellingsen, K., van Noije, T. P. C., Wild, O., Zeng, G.,
950 Amann, M., Atherton, C. S., Bell, N., Bergmann, D. J., Bey, I., Butler, T., Cofala, J., Collins, W. J.,
951 Derwent, R. G., Doherty, R. M., Drevet, J., Eskes, H. J., Fiore, A. M., Gauss, M., Hauglustaine, D. A.,
952 Horowitz, L. W., Isaksen, I. S. A., Krol, M. C., Lamarque, J.-., Lawrence, M. G., Montanaro, V., Müller,
953 J.-., Pitari, G., Prather, M. J., Pyle, J. A., Rast, S., Rodriguez, J. M., Sanderson, M. G., Savage, N. H.,
954 Shindell, D. T., Strahan, S. E., Sudo, K., and Szopa, S.: Multimodel ensemble simulations of present-
955 day and near-future tropospheric ozone. *J. Geophys. Res.*, D08301, doi: 10.1029/2005JD006338, 2006.

956 Strode, S. A., Rodriguez, J. M., Logan, J. A., Cooper, O. R., Witte, J. C., Lamsal, L. N., Damon, M., Van
957 Aartsen, B., Steenrod, S. D., and Strahan, S. E.: Trends and variability in surface ozone over the United
958 States, *J. Geophys. Res.*, 120, 9020-9042, doi:10.1002/2014JD022784, 2015.

959 Tiwari, A. K., Suresh, K. G., Arouri, M., and Teulon, F.: Causality between consumer price and producer
960 price: Evidence from Mexico, *Econ. Model.*, 36, 432-440, doi:10.1016/j.econmod.2013.09.050, 2014.

961 Torres-Jardon, R., García-Reynoso, J. A., Jazcilevich, A., Ruiz-Suárez, L. G., and Keener, T. C.:
962 Assessment of the ozone-nitrogen oxide-volatile organic compound sensitivity of Mexico City through an
963 indicator-based approach: measurements and numerical simulations comparison, *J. Air Waste Manag.*
964 *Assoc.*, 59, 1155-1172, doi:10.3155/1047-3289.59.10.1155, 2009.

965 VanCuren, R.: Transport aloft drives peak ozone in the Mojave Desert, *Atmos. Environ.*, 109, 331-341,
966 doi: 10.1016/j.atmosenv.2014.09.057, 2015.

967 Vingarzan, R.: A review of surface ozone background levels and trends, *Atmos. Environ.*, 38, 3431-3442,
968 doi:10.1016/j.atmosenv.2004.03.030, 2004.

969 Velasco, E., Lamb, B., Westberg, H., Allwine, E., Sosa, G., Arriaga-Colina, J. L., Jobson, B. T.,
970 Alexander, M. L., Prazeller, P., Knighton, W. B., Rogers, T. M., Grutter, M., Herndon, S. C., Kolb, C. E.,
971 Zavala, M., de Foy, B., Volkamer, R., Molina, L. T., and Molina, M. J.: Distribution, magnitudes,
972 reactivities, ratios and diurnal patterns of volatile organic compounds in the Valley of Mexico during the
973 MCMA 2002 & 2003 field campaigns, *Atmos. Chem. Phys.*, 7, 329-353, doi:10.5194/acp-7-329-2007,
974 2007.

975 Wang, Y., Konopka, P., Liu, Y., Chen, H., Müller, R., Plöger, F., Riese, M., Cai, Z., and Lü, D.:
976 Tropospheric ozone trend over Beijing from 2002-2010: Ozone-sonde measurements and modeling
977 analysis, *Atmos. Chem. Phys.*, 12, 8389-8399, doi:10.5194/acp-12-8389-2012, 2012.

978 Wilson, R. C., Fleming, Z. L., Monks, P. S., Clain, G., Henne, S., Konovalov, I. B., Szopa, S., and Menut,
979 L.: Have primary emission reduction measures reduced ozone across Europe? An analysis of European
980 rural background ozone trends 1996-2005, *Atmos. Chem. Phys.*, 12, 437-454, doi:10.5194/acp-12-437-
981 2012, 2012.

982 Wolff, G. T., Kahlbaum, D. F., and Heuss, J. M.: The vanishing ozone weekday/weekend effect, *J. Air*
983 *Waste Manage.*, 63, 292-299, doi:10.1080/10962247.2012.749312, 2013.

984 World Health Organization: Ambient (outdoor) air quality and health, 2014 update,
985 <http://www.who.int/mediacentre/factsheets/fs313/en/>, last access: 21 May 2016.

986 Xing, J., Pleim, J., Mathur, R., Pouliot, G., Hogrefe, C., Gan, C.-M., and Wei, C.: Historical gaseous and
987 primary aerosol emissions in the United States from 1990 to 2010, *Atmos. Chem. Phys.*, 13, 7531-7549,
988 doi:10.5194/acp-13-7531-2013, 2013.

989 Xu, X., Lin, W., Wang, T., Yan, P., Tang, J., Meng, Z., and Wang, Y.: Long-term trend of surface ozone
990 at a regional background station in eastern China 1991-2006: Enhanced variability, *Atmos. Chem. Phys.*,
991 8, 2595-2607, doi:10.5194/acp-8-2595-2008, 2008.

992 Zellweger, C., Hüglin, C., Klausen, J., Steinbacher, M., Vollmer, M., and Buchmann, B.: Inter-comparison
993 of four different carbon monoxide measurement techniques and evaluation of the long-term carbon
994 monoxide time series of Jungfraujoch, *Atmos. Chem. Phys.*, 9, 3491-3503, doi:10.5194/acp-9-3491-
995 2009, 2009.

Zheng, J., Swall, J. L., Cox, W. M., and Davis, J. M. Interannual variation in meteorologically adjusted ozone levels in the eastern United States: A comparison of two approaches, Atmos. Environ., 41, 705-716, doi:10.1016/j.atmosenv.2006.09.010, 2007.

Table 1. Air quality limit values stated in Mexican legislation.

Pollutant	Mexican Official Standard	Limit value*
O ₃ (ppb)	NOM-020-SSA1-1993	110 (1-h), 80 (8-h) ^{a,b}
	NOM-020-SSA1-2014	95 (1-h) , 70 (8-h) ^{a,b}
PM ₁₀ (µg m ⁻³)	NOM-025-SSA1-1993	75 (24-h), 40 (1-yr)
	NOM-025-SSA1-2014	50 (24h), 35 (1-yr)
PM _{2.5} (µg m ⁻³)	NOM-025-SSA1-1993	45 (24-h), 12 (1-yr)
	NOM-025-SSA1-2014	30 (24-h), 10 (1-yr)
CO (ppm)	NOM-02-SSA1-1993	11 (8-h) ^b
NO ₂ (ppm)	NOM-023-SSA1 -1993	0.21 (1-h)

*Average period.

^aNot to be exceeded more than 4 times in a calendar year.

^bRunning average.

Table 2. Site description, location and instrumentation used during 1993 to 2014 within the MMA.

Site	Code	Location	Elevation (m a.s.l.)	Site description
Guadalupe	GPE	25° 40.110' N, 100° 14.907' W	492	Urban background site in the La Pastora park, surrounded by a highly populated area, 450 m from Pablo Rivas Rd.
San Nicolas	SNN	25° 44.727' N, 100° 15.301' W	476	Urban site surrounded by a large number of industries and residential areas, 450 m from Juan Diego Díaz de Beriagna Rd.
Obispado	OBI	25° 40.561' N, 100° 20.314' W	560	Urban site near the city centre of MMA, 250 m from Jose Eleuterio González Rd. and 250 m from Antonio L. Rodríguez Rd.
San Bernabe	SNB	25° 45.415' N, 100° 21.949' W	571	Urban site in a residential area downwind of an industrial area with high traffic volume, 140 m from Aztlan Rd.
Santa Catarina	STA	25° 40.542' N, 100° 27.901' W	679	Urban site downwind of industrial sources, 200 m from Manuel Ordoñez Rd.

1021 **Table 3.** Results for O₃ and O_x long-term trends expressed in ppb yr⁻¹ for 1993-2014 at the 5 sites within
 1022 the MMA by season.

Site	Period	Ozone (O ₃)			Odd oxygen (O _x = O ₃ + NO ₂)		
		ppb yr ⁻¹	% yr ⁻¹	Significance	ppb yr ⁻¹	% yr ⁻¹	Significance
GPE	Annual	0.21	0.78	*	0.31	0.80	**
	Spring	0.24	0.73	*	0.32	0.69	*
	Summer	0.30	1.16	*	0.38	1.18	*
	Autumn	0.14	0.53		0.25	0.62	
	Winter	0.12	0.53		0.14	0.33	*
SNN	Annual	0.33	1.40	***	0.45	1.25	*
	Spring	0.39	1.38	*	0.49	1.22	*
	Summer	0.47	2.24	*	0.58	1.87	***
	Autumn	0.41	1.96	*	0.65	1.94	*
	Winter	0.14	0.68		0.23	0.58	+
OBI	Annual	0.30	1.29	*	-0.17	-0.35	
	Spring	0.43	1.56	*	0.02	0.03	*
	Summer	0.26	0.98	*	-0.04	-0.09	
	Autumn	0.29	1.33	+	-0.66	-1.15	
	Winter	0.25	1.46		-0.28	-0.53	
SNB	Annual	0.19	0.65	+	0.61	1.66	**
	Spring	0.37	1.07	+	0.67	1.65	+
	Summer	0.31	1.06	***	0.66	2.17	***
	Autumn	0.19	0.64		0.60	1.61	+
	Winter	0.02	0.07		0.47	1.12	+
STA	Annual	0.01	0.01		-0.15	-0.28	
	Spring	-0.04	-0.11		-0.01	-0.02	
	Summer	0.09	0.28		0.13	0.27	
	Autumn	0.00	0.00		-0.22	-0.41	
	Winter	-0.09	-0.43		-0.63	-1.15	*

1023 ⁺Level of significance $p < 0.1$.
 1024 ^{*}Level of significance $p < 0.05$.
 1025 ^{**}Level of significance $p < 0.001$.
 1026 ^{***}Level of significance $p < 0.001$.
 1027

1028
 1029
 1030
 1031
 1032
 1033

1034 **Table 4.** Results for O₃ and O_x long-term trends by season expressed in ppb yr⁻¹ during 1993-2014 for
 1035 the MCMA and MMA, and during 1996-2014 for the GMA.

Urban area	Period	Ozone (O ₃)			Odd oxygen (O ₃ + NO ₂)		
		ppb yr ⁻¹	% yr ⁻¹	Significance	ppb yr ⁻¹	% yr ⁻¹	Significance
MCMA	Annual	-1.15	-2.04	***	-1.87	-1.94	***
	Spring	-0.97	-1.53	***	-1.77	-1.71	***
	Summer	-0.97	-1.88	***	-1.44	-1.67	***
	Autumn	-1.12	-2.20	***	-1.89	-2.15	***
	Winter	-1.62	-2.64	***	-2.47	-2.27	***
GMA	Annual	-0.29	-0.81		-1.46	-1.85	+
	Spring	-0.26	-0.57		-1.89	-2.07	*
	Summer	-0.10	-0.32		-1.43	-1.89	*
	Autumn	-0.09	0.33		-1.40	-1.97	*
	Winter	-0.34	-1.01		-1.74	-2.08	***
MMA	Annual	0.22	0.84	**	0.13	0.30	
	Spring	0.32	1.04	**	0.29	0.63	
	Summer	0.27	0.99	***	0.28	0.72	***
	Autumn	0.25	1.03		0.13	0.31	
	Winter	0.10	0.45		0.01	-0.01	

1036 ⁺Level of significance $p < 0.1$.
 1037 ^{*}Level of significance $p < 0.05$.
 1038 ^{**}Level of significance $p < 0.001$.
 1039 ^{***}Level of significance $p < 0.001$.
 1040

1041
 1042
 1043
 1044
 1045
 1046
 1047
 1048
 1049
 1050
 1051
 1052
 1053
 1054

1055
1056

Table 5. Results for O₃ daily maxima long-term trends by season in ppb yr⁻¹ during 1993-2014 at the 5 sites within the MMA.

Site	Period	Ozone (O ₃)		
		ppb yr ⁻¹	% yr ⁻¹	Significance
GPE	Annual	0.45	1.02	**
	Spring	0.48	0.94	**
	Summer	0.64	1.50	*
	Autumn	0.35	0.74	
	Winter	0.26	0.63	
SNN	Annual	0.79	2.13	***
	Spring	0.87	2.01	***
	Summer	0.85	2.42	***
	Autumn	0.93	2.73	*
	Winter	0.44	1.29	
OBI	Annual	0.65	1.51	*
	Spring	0.78	1.62	**
	Summer	0.53	1.10	*
	Autumn	0.75	1.77	
	Winter	0.21	0.55	
SNB	Annual	0.40	0.80	***
	Spring	0.85	1.58	***
	Summer	0.67	1.36	***
	Autumn	0.52	1.05	*
	Winter	0.05	0.10	
STA	Annual	0.01	-0.01	
	Spring	-0.05	-0.09	
	Summer	0.22	0.35	
	Autumn	-0.07	-0.12	
	Winter	-0.35	-0.75	+

1057
1058
1059
1060
1061

+Level of significance $p < 0.1$.
*Level of significance $p < 0.05$.
**Level of significance $p < 0.001$.
***Level of significance $p < 0.001$.

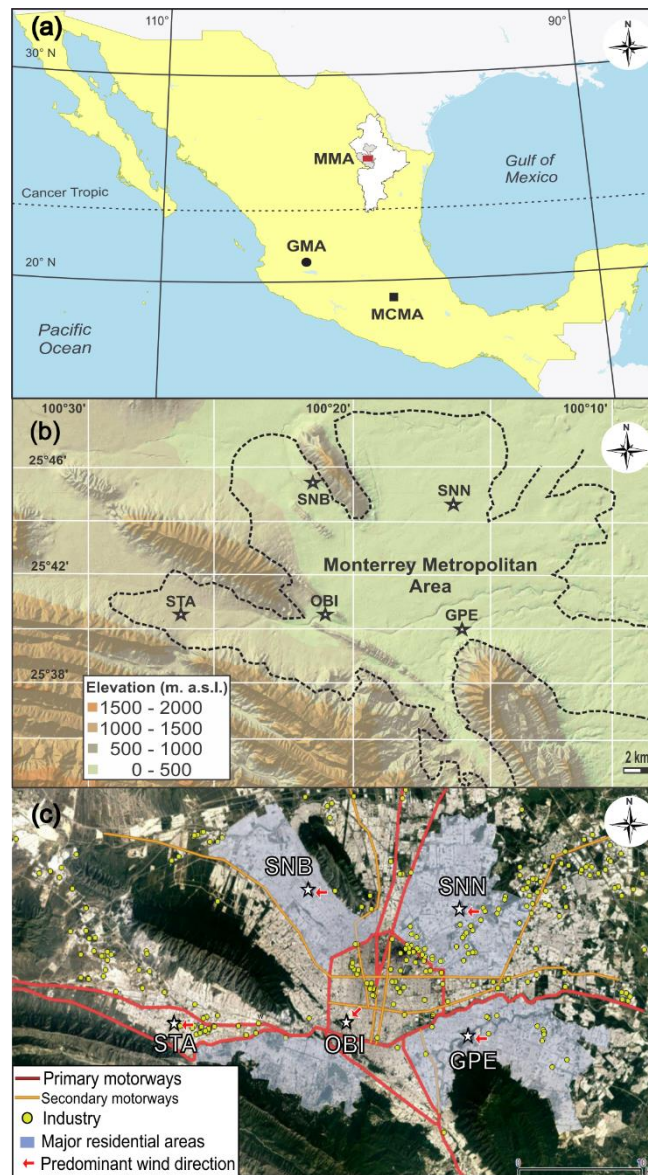


Fig. 1(a). The MMA, MCMA and GMA in the national context. **(b).** Topography of the MMA and distribution of the 5 monitoring sites over the area. **(c).** The 5 monitoring sites in relation to primary and secondary motorways, industries and major residential areas. The red arrows show the predominant wind direction at each site during 1993 to 2014.

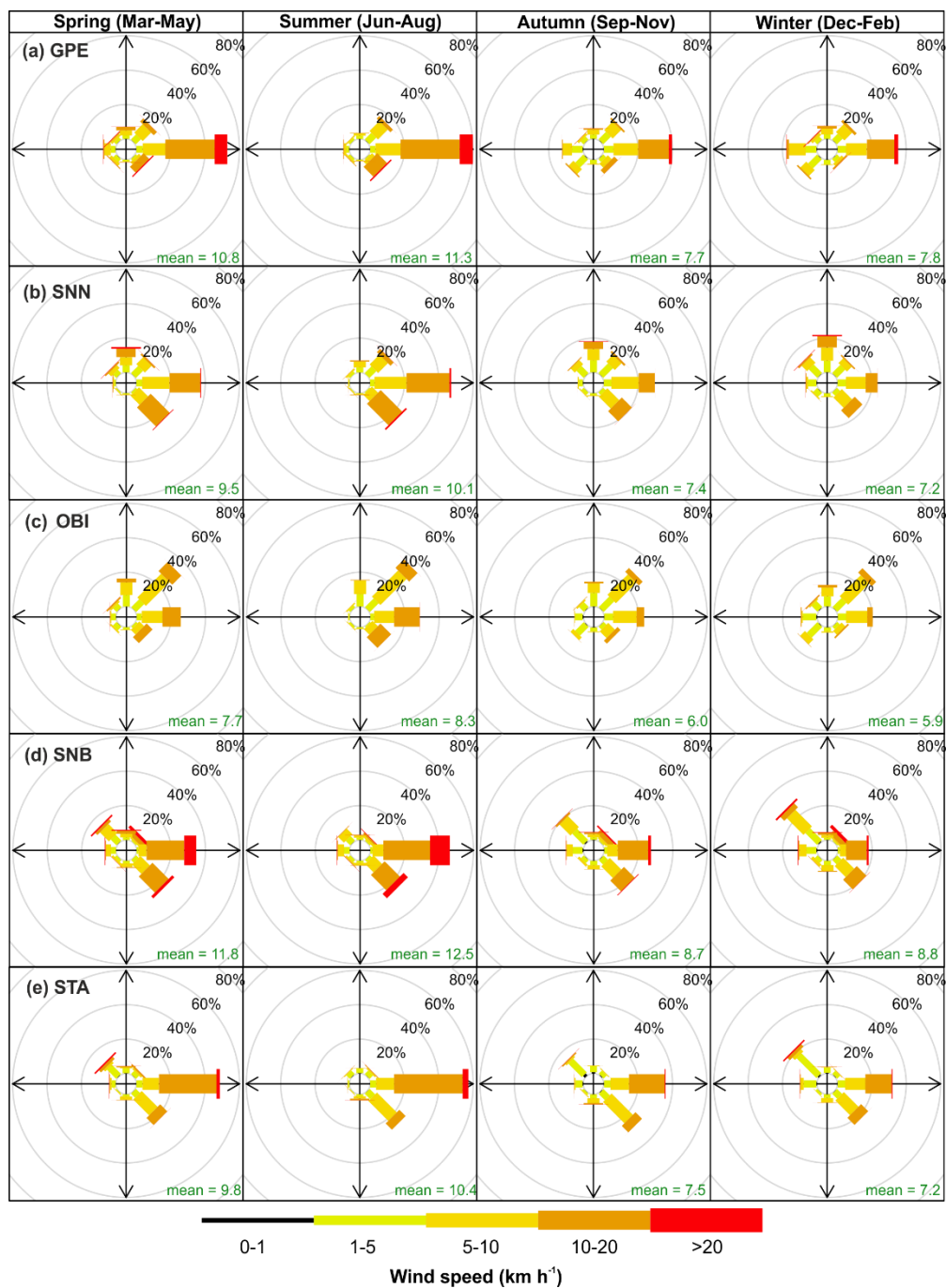


Fig. 2. Frequency of counts of measured wind direction occurrence by season and site within the MMA during 1993-2014.

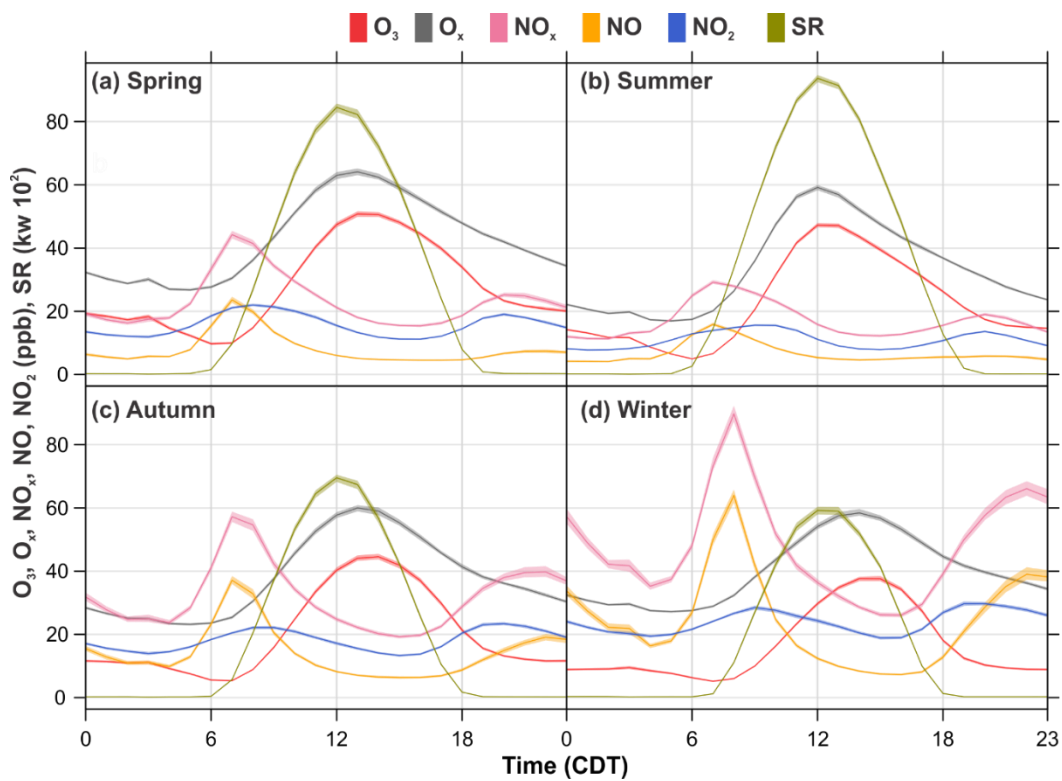


Fig. 3. Seasonal average daily profiles for O_3 , O_x , NO_x , NO , NO_2 and SR within the MMA during 1993-2014. The shading shows the 95 % confidence intervals of the average.

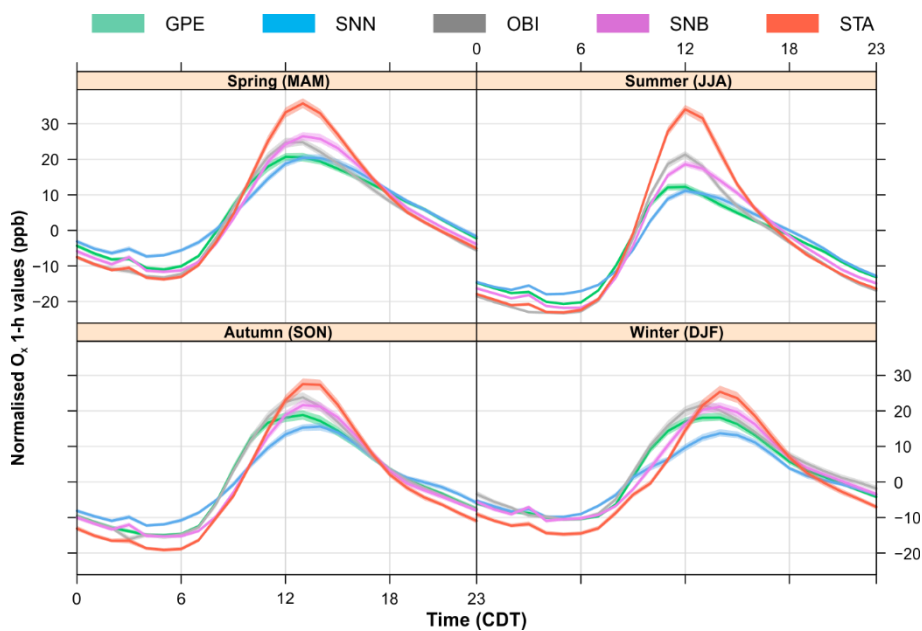


Fig. 4. Seasonal O_x de-trended daily profiles within the MMA during 1993-2014. De-trended O_x daily cycles were constructed by subtracting daily averages from hourly averages to remove the impact of long-term trends.

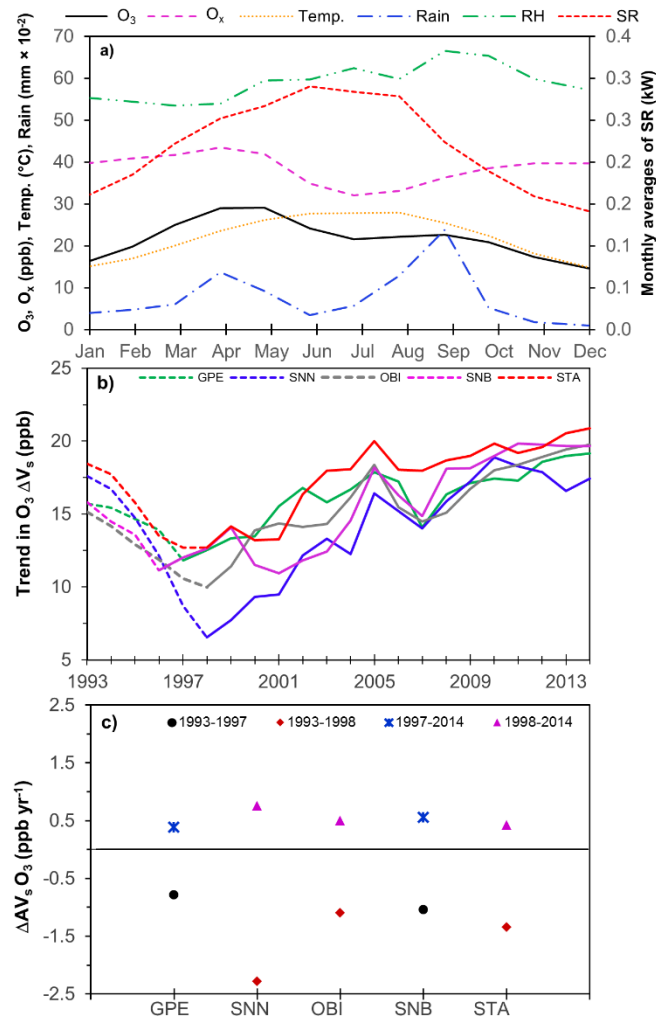


Fig. 5a). Annual cycles of O_3 , temperature, rainfall, RH and SR constructed by averaging records from 1993 to 2014 for a 1-year period. **b).** Trends in AV_s of O_3 recorded at the 5 monitoring sites within the MMA from 1993 to 2014. The decline in AV_s observed is due to the economic crisis experienced in Mexico during 1994-1996, followed by persistent increases in AV_s since 1998. **c).** Annual rates of change in O_3 AV_s by site, before and after the 1994-1996 economic crisis.

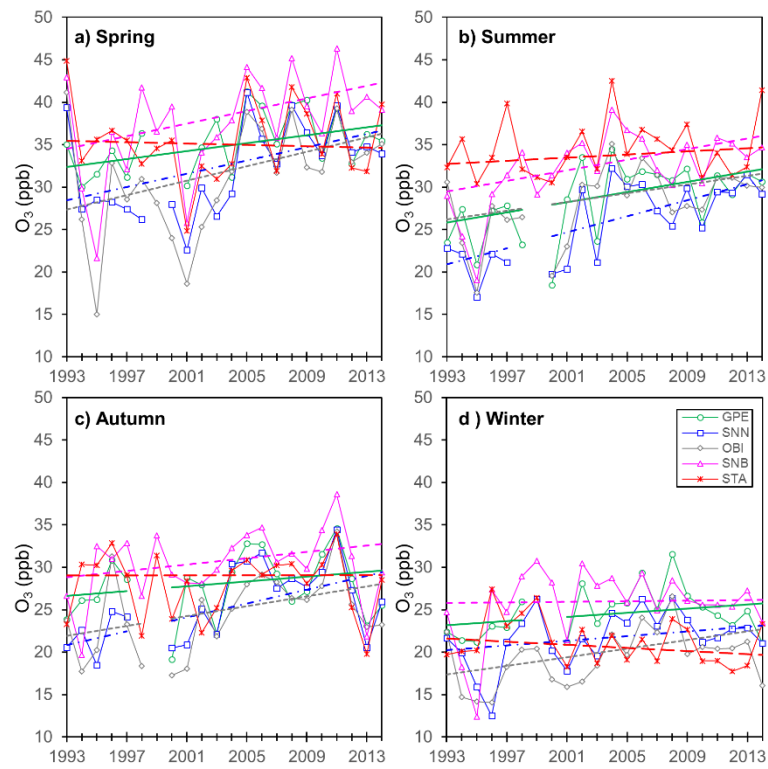


Fig. 6. Seasonal trends of O_3 within the MMA during 1993-2014. Each data point represents the average of the 3-month period that defines the season. The continuous lines show the Sen trend.

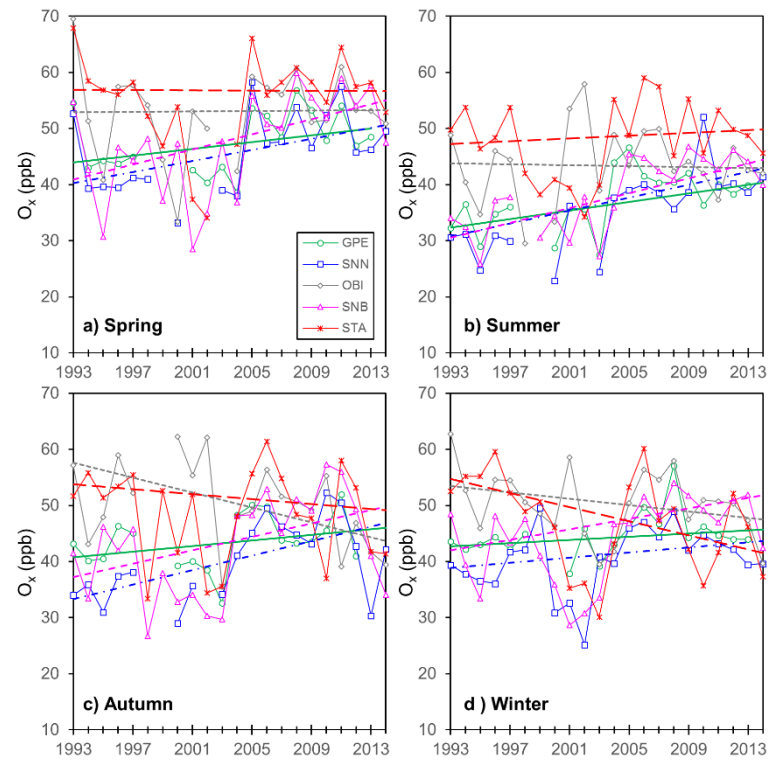


Fig. 7. Seasonal trends of O_X within the MMA during 1993-2014. Each data point represents the average of the 3-month period that defines the season. The continuous lines show the Sen trend.

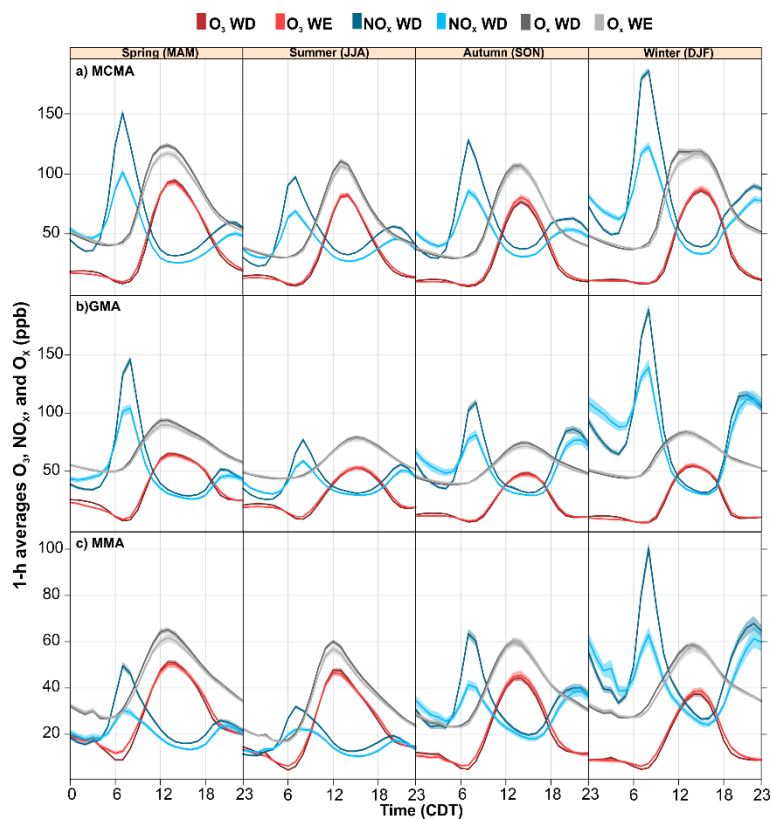


Fig. 8. Seasonal average diurnal cycles of O_3 , O_X and NO_X during 1993-2014 for the MCMA and the MMA, and between 1996-2014 for the GMA. The shading shows the 95% confidence intervals of the average, calculated through bootstrap resampling (Carslaw, 2015).

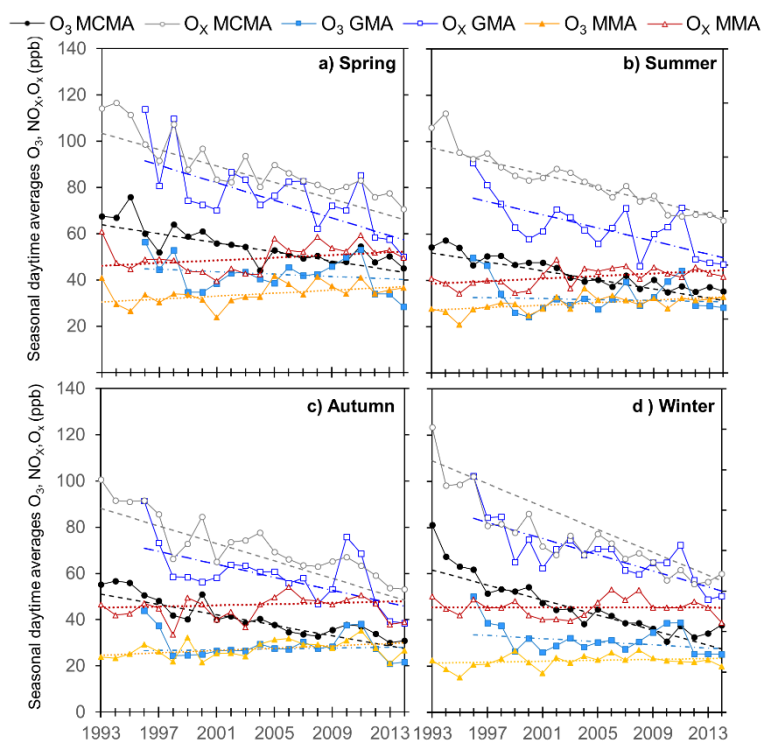


Fig. 9. Seasonal trends in O_3 and O_X for the MCMA and MMA during 1993-2014, and for the GMA during 1996-2014. Each data point represents the average of the 3-month period that defines the season. The dashed lines show the Sen trend.

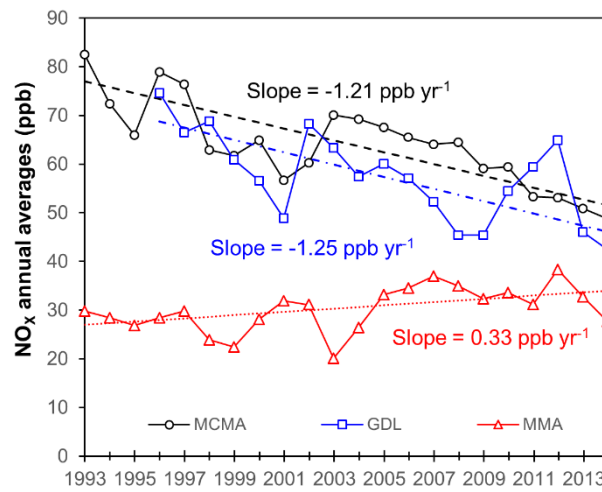


Fig. 10. Trends for NO_x at the MCMA and MMA during 1993-2014, and at the GMA during 1996-2014. The dashed lines represent the Sen slopes. All trends are statistically significant at $p < 0.05$.

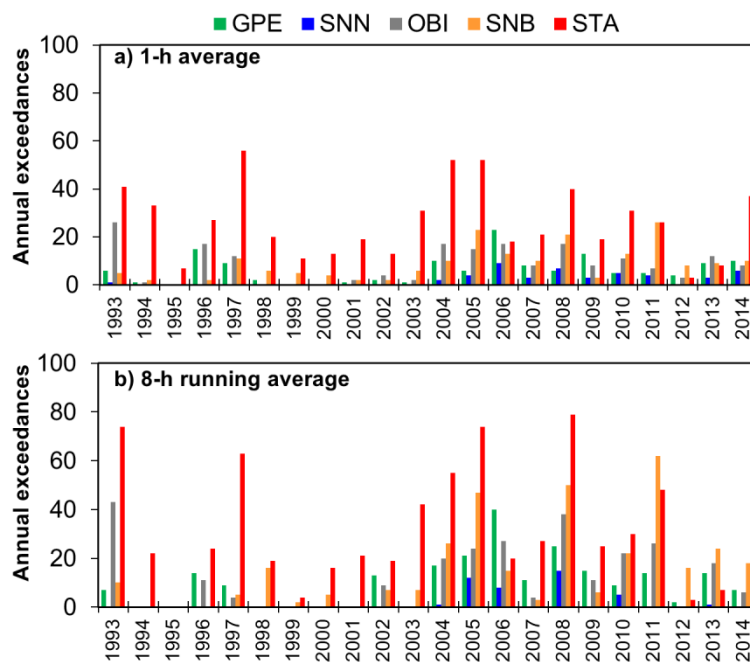


Fig. 11. Annual exceedances of the O_3 NOM for 1-h averages (110 ppb) and 8-h running averages (80 ppb) at the 5 monitoring sites within the MMA from 1993 to 2014.

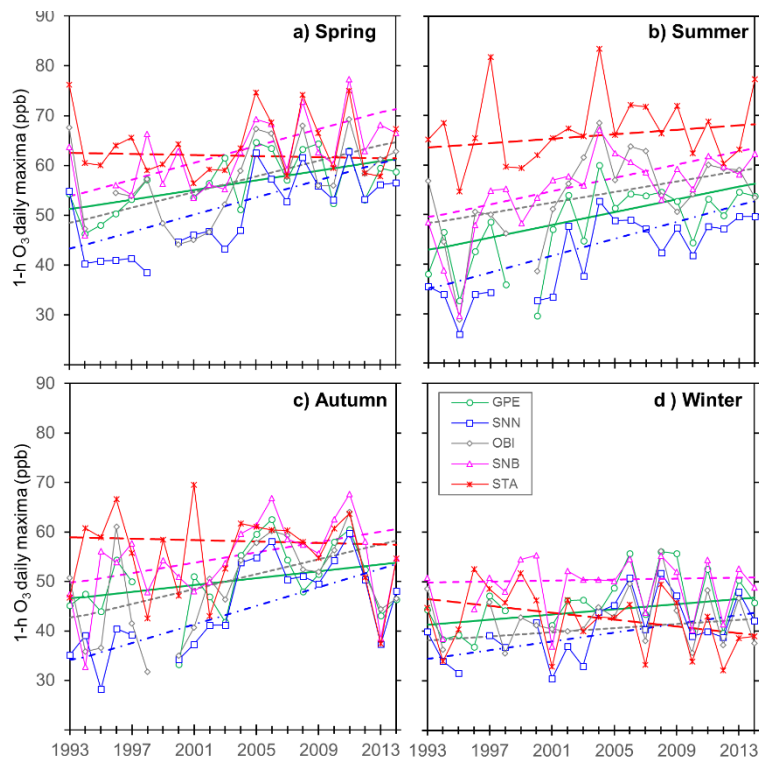


Fig. 12. Seasonal trends in 1-h O₃ daily maxima at the MMA during 1993-2014. Each data point represents the average of the 3-month period that defines the season. The dashed lines show the Sen trend.

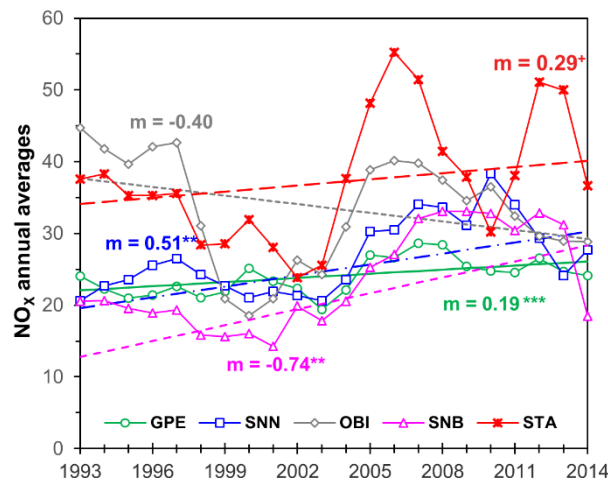


Fig. 13. Long-term trends for NO_x at the 5 monitoring sites within the MMA during 1993-2014. The dashed lines represent the Sen slopes. Annual NO_x rates of change are described as m for slope and expressed in units of ppb yr⁻¹. Levels of confidence are represented as $^+ = p < 0.1$, $^* = p < 0.05$, $^{**} = p < 0.001$, $^{***} = p < 0.001$.